T.C.

ALTINBAS UNIVERSITY

Institute of Graduate Studies

Electrical and Computer Engineering

A NOVEL DESIGN RECONFIGURABLE ANTENNA BASED ON THE METAMATERIAL FOR WEARABLE APPLICATIONS

Mohaimen Qahtan AL-GBURI

Master of Science

Supervisor

Asst. Prof. Dr. Muhammad Ilyas

Istanbul, 2021

A Novel Design Reconfigurable Antenna Based on the Metamaterial for Wearable Applications

by

Mohaimen Qahtan Al-Gburi

Electrical and Computer Engineering

Submitted to the Graduate School of Science and Engineering

in partial fulfillment of the requirements for the degree of

Master of Science

ALTINBAŞ UNIVERSITY

2021

The thesis titled "A NOVEL DESIGN RECONFIGURABLE ANTENNA BASED ON THE METAMATERIAL FOR WEARABLE APPLICATIONS" prepared and presented by "Mohaimen Qahtan AL-GBURI" was accepted as a Select Degree Thesis in Electrical and Computer Engineering.

____

Asst. Prof. Dr. Muhammad Ilyas

Supervisor

Thesis Defense Jury Members:

Asst. Prof. Dr. Muhammad ILYAS	School of Engineering and Natural Sciences, Altinbas University	_________________
Asst. Prof. Dr. Çağdaş ATİLLA	School of Engineering and Natural Sciences, Altinbas University	_________________
Asst. Prof. Dr. Çağatay AYDIN	Faculty of Engineering, Ege University	_________________

I certify that this thesis satisfies all the requirements as a thesis for the degree of Master of Science.

Approval Date of Institute of Graduate Studies ___/____/____

I hereby declare that all information in this document has been obtained and presented in accordance with academic rules and ethical conduct. I also declare that, as required by these rules and conduct, I have fully cited and referenced all material and results that are not original to this work.

Mohaimen Qahtan Al-Gburi

DEDICATION

I would like to thank Allah Almighty for my success in my studies ,my dear father and my teacher, leader and inspiration , my dear mother ... my dear brothers ... my dear sister.., my dear friends and everyone who stood beside me, I thank you very much .

ACKNOWLEDGEMENTS

I would like to thank very much to my supervisor, Assistant Professor Dr. Muhammad Ilyas for his assistance throughout the research period and for answering many questions and he was the best help for me throughout the study period. Without his time and help, this research would not have been completed and I am very grateful to him.

ABSTRACT

A NOVEL DESIGN RECONFIGURABLE ANTENNA BASED ON THE METAMATERIAL FOR WEARABLE APPLICATIONS

Al-gburi, Mohaimen Qahtan,

M.Sc, Electrical and Computer Engineering, Altınbaş University,

Supervisor: Asst. Prof. Dr.Muhammad Ilyas

Date: 29/7/2021

Pages: 92

A novel design of wearable antenna depending on metamaterials inspired-fractal Minkowski-shaped for industrial, scientific, and medical (ISM) applications is presented. The antenna consists of a conventional monopole and a Chebyshev transformer coupled with a unit cell of a fractal Minkowski curve to obtain three bands covering the ISM and Wireless Local Area Network (WLAN) applications. To enhance the antenna performance, the authors proposed the Electromagnetic Band Gap (EBG) layer of 3×4 array is introduced into the design structure. The authors used material FR4 dielectric as a substrate to design the antenna with dimensions of 51mm x 45mm x 1.6mm and fed by a 50 Ω port. The Antenna performance is analyzed numerically using CST Microwave Studio (CSTMWS) depending on the Finite Integral Technique (FIT). Various investigation analyses have carried out to verify optimum antenna performance. The proposed antenna realizes reconfiguration by using the PIN diode. In both cases (switching= ON, OFF) the antenna achieves good bandwidth, $|S_{11}|$<-10dB, and excellent impedance matching.

Keywords: Metamaterial, EBG, Printed-Circuit Antenna, End-Fire

TABLE OF CONTENTS

Pages

LIST OF TABLES

Pages

LIST OF FIGURES

Pages

LIST OF ABBREVIATIONS

WHMS	:	Wearable Health Management Systems.
IoT	:	Internet of Things
PAN	:	Personal Area Network
FSK	:	Frequency Shift Keying
ISM	:	Industrial, Scientific, and Medical
WBAN	:	Wireless Body Area Network
IEEE	:	Institute of Electrical and Electronics Engineers
EBG	:	Electromagnetic Band-Gap
CPW	:	Coplanar Waveguide
CSTMWS	:	CST Microwave Studio
MAC	:	Media Access Control
RBF	:	Reject Band Filter
WSN	:	Wireless Sensor Networks
IP	:	Internet Protocol
SAR	:	Specific Absorption Rate
NRI	:	Negative Refractive Index
MOL	:	Minkowiski Open Loop
OST	:	Open - Stup Transmission Line

CNT	:	Carbon Nanotube Patch
IL	:	Insertion loss
RL	:	Return Loss
GPS	:	Global Position System
WLAN	:	Wireless Local Area
SIR	:	Stepped-Impedance Resonator
SIW	:	Substrate-integrated waveguide resonator
WLAN	:	Wireless Local Area Network
UWB	:	Ultra-wide band
VHF	:	Very high frequency
UHF	:	Ultra-high frequency
RF	:	Radio frequency

LIST OF SYMBOLS

μ	:	Mobility of electron
λ	:	Wave length
ω	:	Angle frequency

1. INTRODUCTION

1.1 OVERVIEW

Recently, the miniaturization of electronics has led to increased demand for wearable devices that can be connected to the body of users [1]–[3]. Wearable Health Management Systems (WHMS) is to be among the most growing fields of study and research. In latest years, we have seen wearable devices that can function well enough to replace our instrument with a range of medical apps, smart clothing which recognizes the vitals of a human body, make decisions based on results. In order to make these matters potential, research has been led to make antennas quite adequate in the devices. To employ the wearable system in healthcare applications, the antenna requires particular consideration when developing. Weight, size, power consumption, conformity, and Flexibility are the biggest problems and constraints that should be solved [4]–[5]. Many researchers have been tried to developed studies for suitable designs for microstrip wearable antenna that be lightweight, flexible, and conformable with the human body. Wearable systems can be utilized for disaster and evacuation management services, including raincoats, gloves, boots, and helmets [6].

In current times, great interest has arisen in flexible / semi-flexible wearable devices for telemedicine and biomedical applications. Much attention is paid to the use of flexible/semi-flexible materials for the production of wearable nodes [7]. With the great advancement in the technology of wearable antennas, developed has been observed utilize of implantable devices in various fields for healthcare applications such as; intracranial pressure monitoring [8], glucose monitoring [9], neurological recording [10], and Endoscopy [11]–[12]. Operate the antenna at a good range and minimizing the dimension of wearable devices while maintaining its high efficiency is one of the issues facing researchers. To address these problems, various efforts have been made to reduce the size of the wearable antenna, such as reactive loading [9], utilize materials that high permittivity [13], quarter mode designs [14], shorting pins [15], and enhance the resonator length in order to increase the current path [16]. When the mentioned techniques are applied, the size of the antenna is significantly reduced. Nevertheless, there are Difficulties that appear such as narrow bandwidth, complex designs, and low gain. Also, new communication system architecture tends to be used simple designs free from complexity along with ultra-compact components [17]–[18]. Designing an antenna with these specifications is a difficult mission to implement. There is a growing disparity between health care providers and patients, this imbalance puts substantial pressure on the health sector [19]. In order to meet the challenges of modern healthcare, wearable devices are used, which helps the health sector and patients to better and safely manage their resources. Day after day, the use of remote surveillance in healthcare shows great possibilities as it is lightweight and easy to perform especially favorable for housebound patients, elderly and frail [20]. Moreover, it offers an important method for tracking chronic condition patients by a continuous evaluation of signs and symptoms of the disease [21]. The demand for wearable devices has constantly increased and has become more important due to their high reliability in monitoring and tracking during various sporting activities, and training has become more significant for monitoring. It is worth noting that wearable antennas that work on-body if their size is small, the efficiency of the antenna decrease. To maintain high efficiency and performance, a balance should be made between parameters such as bandwidth, radiation pattern, and return loss.

Day after day increases the demand and needs for these antennas to be portable, compact, low-cost, lightweight, needless setup, and maintenance-free. Notably, the patch antenna is one of the essential studies attentions of wearable antennas for WBAN applications [22] due to the relatively high directivity and wide ground plane used in its construction. This shows us, that microstrip patch antennas have many benefits and features for wearable devices on the body. The three most important elements are cost-effectiveness, the relative separation, simplicity of design is provided by using the ground level between the surface and the radiating side, resulting in a significant reduction in the energy wasted by the skin. [23].

On the other hand, due to the properties of human tissues that have high permittivity, when the human body is exposed to electromagnetic waves that radiate from the wearable antenna, it absorbs a large amount of this energy. Therefore, the parameters of the wearable antenna are decreased noticeably during its functional near of Human body, this causes significant problems in the wireless communication field. Furthermore, electromagnetic waves absorbed by the human body have undesirable environmental and biological impacts [24]. In this thesis, a novel design of wearable antenna depending on metamaterials inspired-fractal Minkowski-shaped for ISM and WLAN applications is presented.

1.2 OVERVIEW OF FRACTAL-BASED SLOT ANTENNAS

Common fractal geometry methods including Minkowski, Koch, Hilbert, Sierpinski, Cantor as well as other fractal curves were effectively utilized for producing multi and dual-band printed slot antennas for different wireless applications. In that regard, applications related to fractal geometry in designing slot printed antennas could be categorized into two types. In the first one, direct fractal geometry application was used. In such a situation, all antenna slot structures are made by fractal geometries. The multi- and performance related to these antennas were extracted almost directly with no necessity for slot shape modification or tuning elements. In the second one, slot structures are considered as a combination related to Euclidian structures, including rectangle, square, triangle, and additional polygons, in addition to fractal geometry that is superimposed on such structures, in which all line segments will be replaced via fractal curve with a specific level of iteration. Fractals produced by several Euclidean geometries including triangle, circle, and others, were used for producing dual-band antennas for many applications related to the communication field.

2. LITERATURE SURVEY

With the rapid and increasing demand for wearable and portable devices greatly in recent years, this leads to the imperative of planning and designing microwave resonators that can work with various cutting frequencies at the same time. There are several methods used to generate multiple ranges, including the use of fractal geometry, metamaterial, EBG, and others, here we explain some previous studies in this regard:

- **In 2016 Seevan F et al.** [25] A dual-band antenna based on a square-shaped fractal Cantor structure is designed for use in WiMAX, WLAN, and ISM band applications. The antenna structure was developed by combining the third iteration of Cantor's square fractal geometry, etching the resonator structure, and modify the ground plane, to increase the antenna impedance and enhance matching with provide the desired radiation characteristics. The antenna was simulated using CST software. The results show that the antenna behavior was omnidirectional, dual-band resonant 42% (2.35-3.61 GHz) at 2.45 GHz and 20% (5.15-6.25 GHz) at 5.8 GHz. The antenna at the lower resonant band had a gain of 2.8–3.5 dB and at the upper resonance of 3.7–4.3 dB. The antenna is printed on a 50mm x 50mm FR4 dielectric substrate with a thickness of 1.6mm. The antenna covered a wide range of frequencies for wireless communication system applications.

- **In 2017 Dalfiah.J and Dabu Karuppasamy** [26] a monopole circular antenna based on a Split-Ring Resonator (SRR) is designed to operate for industrial, scientific, and medical (ISM) bands. (SRR) works as a resonator developed by performing the slotting process using split rings to achieve UWB. The SRR consists of two conductive rings, each with a slot opposite the other, and separated by a gap. In order to increase the antenna impedance, a stub was used. To improve the antenna performance, parametric studies were carried out on different numbers of stubs, various ring structures, and different lengths of ground plane. The antenna was fed with a coplanar waveguide (CPW) and simulated by (ADS) software. The antenna was printed on dielectric substrate FR4 Glass Epoxy material. The ground plane has been modified to realize a resonant frequency at 2.45 GHz with a bandwidth of 100 MHz and radiation efficiency at 50%. The antenna was appropriate for WBAN applications for short-term communication.

- **In 2017 Omar Masood Khan et al.** [27] A compact monopolar fractal antenna is designed for (WBAN) applications, the antenna structure has been developed by integrating a second-order flamenco-shaped fractal geometry with ground plane defects to achieve resonance that covers the (ISM) bands. The antenna was fed by a microstrip transmission line 50 ohm port with SMA connector. The antenna was printed on dielectric substrate Rogers RT 5870 measuring 20 mm x 27.14 mm with a thickness of 1.575 mm. Antenna simulated using a CST Microwave Studio package. The patterns of radiation, gain, and resonant frequency were investigated and found suitable for wearable off-body. The antenna covers the frequencies of 2.4-2.48 GHz and the peak gain of 1.24 dBi with the Omni-directional pattern that provides appropriateness for wireless communication.

- **In 2019 Sourav Roy and Ujjal Chakraborty** [28] a compact, wide-band wearable antenna based on fractal metamaterials is designed to operate On-body area applications. The unit cell structure resonator work as a radiator for the wearable antenna which is excited directly by a 50-ohm line from the ground plane to the resonator. The fractal metamaterial was printed on a substrate of jeans material which is flexible and low cost, the overall size of the wearable antenna has 60 × 60 × 2 mm3. The antenna structure had analyzed using the HFSS 14 software, and the antenna performance was examined in bending scenarios and their effect on the human body areas. The dual-band antenna achieved a wide measured bandwidth of about 49.11% (4.24-7 GHz) in the upper band and 46% (1.6-2.56 GHz) in the lower band, with the maximum gain of the wearable antenna 5.2 dB at 5.8 GHz and 1.8 dB at 2.4 GHz.

- **In 2019 Hayder S. Ahmed and Elwi** [29] in this work, a fractional antenna at 2.45GHz was designed to reduce mutual coupling and improve antenna performance for Wi-Fi applications. Two monopoles are used separately fed to the 50-ohm type an (SMA) port, and to reduce the mutual coupling between the monopoles, a reject band filter (RBF) was utilized. The proposed RBF was developed by adding an open-stub transmission line coupled with Minkowski-shaped cell open-loop resonators in order to obtain a zero refractive index response. A significant reduction in mutual coupling was achieved by integrating two RBF cells, and the surface impedance increased at 2.45 GHz to match with Wi-Fi applications. The antenna was simulated using HFSS and CST software packages. The gain of the antenna was found to be around 2 dBi at 2.45 GHz. The antenna is printed on an FR-4 dielectric substrate placed on a full copper ground plane.

- **In 2019 Ali Arif et al.** [30] a low-profile, compact triangular wearable antenna based on Koch fractal geometry has been introduced for (WBAN) applications. The antenna structure was developed by integrating defective ground structure, meandering slits, and Koch fractal geometry. The fractal antenna was printed on flexible dielectric substrate low-cost Roger RT / duroid 5880 dimensions of 39mm x 39mm x 0.508mm. Bottom side, the ground plane is defective with six slits with truncated corners from copper. The antenna structure was analyzed by CST Microwave Studio package and fed with a 50-ohm inset feed line. The antenna performance was measured in bending scenarios at respected positions and different areas of the human body. The Specific Absorption Rate (SAR) is evaluated and found that within the safety and health limits by the US and EU. Results are 0.26Watt at leg position and 0.34Watt at arms position, according to the standards set by the EU. The fractal antenna achieved a peak gain of 2.06 dB, the center frequency of 2.45 GHz and S11 <-10 dB, along with a bandwidth of 7.75%, and an overall radiation efficiency of 75%. The antenna fabrication showed agreement between experimental and numerical results. Also, the performance of the antenna was good and suitable for WBAN applications.

- **In 2020 Zainab Al-Dulaimi et al.** [31] in this work, a fractal antenna structure array with (EBG) based on Hilbert-shaped metamaterial was designed for MIMO applications. The meander monopole antenna was fed a 50 ohm SMA port. Two monopoles meander structures were printed and placed on an FR4 dielectric substrate, and the ground plane was etched with (EBG) Hilbert-shaped inclusions of the third order, to achieve surface wave reflection away from the antenna elements by having a negative refractive index (NRI). This property occurs when EBG slots are integrated with the EBG defect. Antenna simulated using a CST Microwave Studio package. The antenna achieved an excellent bandwidth at least 25% with S11 <-10 dB and gain of 2.1dBi at 2.45 GHz. The axial ratio of the antenna is less than 3 dB at 2.45 GHz, however, it has achieved circular polarization due to the effects of the EBG structure. The antenna dimensions are 40 mm x 50 mm with a thickness of 1.6 mm.

- **In 2020 Arka Bhattacharyya et al.** [32] Dual-band fractal antenna is designed for biomedical and GPS applications. The antenna was fed with a 50-ohm microstrip-line and printed on a Rodgers 5880 dielectric substrate with a thickness of 1.52 mm. The authors chose the resonator as Minkowski-shaped for their works due to ease of fabrication and simplicity to the iteration. The resonator was developed from Theory of Characteristic Modes (TCM) to achieve two different characteristics of polarization, circular polarization at 1.5 GHz and linear polarization at 2.45 GHz. The antenna was simulated using FEKO software.

- **In 2020 Ali Arif et al.** [33] a wearable fractal antenna triangular-shaped based on Koch structure backed with an (EBG) plane was designed for communications devices applications. The monopole antenna consists of a triangular radiator inspired by Koch structure geometry with an array of EBG 2 × 2 square shapes as an electromagnetic wave reflector in order to increase the isolation between the human body and the antenna. The antenna was mounted on a semi-flexible Rogers 5880 substrate with a thickness of 0.508 and dimensions of 41 x 41 mm2, and an EBG layer of 2 x 2 was printed on the same Rogers 5880 substrate with overall dimensions of 83 x 83 mm2 with a thickness of 1.570 mm. the antenna simulated using CST Microwave Studio. The results showed that adding EBG plane improved the antenna gain to 7.8 dBi, and radiation efficiency 85%, and increased FBR by 16 dB. The center frequency at 2.38 GHz and $S_{11} < -10$ dB, along with a bandwidth 50MHz. The antenna covers the entire MBAN range (2.36-2.40GHz) for on and off-body communications devices.

- **In 2020 Elwi and Sarah G. Abdulqader** [34] a low-profile fractal antenna based on the metamaterial has been introduced in the context of wearable devices operating in wireless power harvesting applications. The antenna consists of an array 3 x 5 of Hilbert-shaped iteration, a unit cells arranged on a rectangular patch. The antenna is printed on a FR4 dielectric substrate dimensions of 28 mm x 32 mm x 0.394 mm, on the other side the ground plane has square defects in the (EBG). The antenna was printed on a self-powered solar panel by solant-rectenna output terminals, and two prototypes of copper and silver nanoparticles (SNPs) were constructed. It was found that the proposed solant-rectenna antenna coverage range is from 0.8 GHz to 10 GHz. In order to create a rectenna port that collects RF energy and converts it into DC voltage at 0.915 GHz, a solant RF port is connected to a rectifier circuit. It was also noted that the proposed rectenna conversion efficiency is 90% and output DC voltage of 1.42V at 0.915 GHz. In this research, the wearable antenna based on solant–rectenna has two sources of clean energy harvesting were obtained from solar and RF energy in one port.

- **In 2021 Sarah M. Obaid et al.** [35] this work presents the design of a fractal Minkowski-shaped antenna based on the metamaterial for biomedical applications. The antenna uses a microwave resonator to measure the blood glucose level of individuals with diabetes. The antenna consists of a four-unit cell from the (MOL), coupled with an (OSTL) to increase the impedance matching and achieve the resonance frequency at 2.45GHz. In order to improve the measurement quality of the blood sample, a multi-walled carbon nanotube (CNT) patch is placed in the middle path of the OSTL to increase the concentration of EMF on the material sample. The proposed sensor is dependent on impedance matching change, bandwidth variation, resonant frequency tuning, and phase displacement S11or S12 spectra, to detect the blood glucose by placing the specimen on the CNT patch. The antenna was printed on FR-4 dielectric substrate 50 mm x 25 mm with resonator simulation using a CST Microwave Studio.

In all previous studies, the ease of design and the use of inexpensive and available materials have not been considered, some of which are large antenna dimensions not suitable for use in pressurized environments. But with minimal justifications and details. Moreover, the use of artificial intelligence algorithms invoke is still very limited in the former characterization methods that are related to such research.

2.1 THESIS OUTLINES

The thesis consists of five chapters, demonstrated as follows:

- **Chapter One:** The overview of antennas and the uses of fractal geometry in designing antennas.
- **Chapter Two:** A literary survey show previous studies in this field.
- **Chapter Three:** Includes the theoretical background about microstrip antenna and feeding methods, benefits and limitations of each type, moreover, demonstrate the characteristics of antennas and the theory of microstrip resonators.
- **Chapter Four:** Covers the unique characteristics of fractal geometry along with the most commonly used fractal geometries applied in designing antennas.
- **Chapter Five:** Presents simulations and discussions of design methodology and parametric studies to obtain optimal conditions to design a wearable antenna based on Metamaterials for biomedical applications.
- **Chapter Six:** Presents the results of the antenna design methodology.
- **Chapter Seven:** Demonstrates the conclusions and suggestions for future work.

3. THEORETICAL BACKGROUND OF MICROSTRIP ANTENNAS

3.1 INTRODUCTION

This chapter provides an overview of microstrip antennas and their applications in wireless communication. This includes this involves the weaknesses and capabilities related to such antennas in various wireless applications. The main parameters affecting antenna performance were studied along with design equations related to the microstrip patch antenna. The frequently used antenna feed approaches were assessed.

3.2 MICROSTRIP ANTENNAS (MSA)

In 1952, the MSA concept was suggested by Deschamps. Nevertheless, in the 70s, Howell and Munson developed practical antennas [36]. The many features of MSA, like the simplicity of fabrication through the use of printed-circuit technologies, small volume, lightweight, resulted in designing numerous configurations for many implementations. With rising necessities for mobile and personal communications, the need for low profile and smaller antenna brought microstrip antennas to the front. The radiation from MSA might happen from fringing fields between ground planes and patch periphery. Length L regarding the rectangular patch for fundamental mode excitation of TM10 is little less than $\lambda/2$, with the wave-length in the dielectric medium is λ, in relation to the free space wave-length λo is specified as $\lambda o / \sqrt{\varepsilon e}$, here εe can be defined as the effective dielectric constant related to microstrip line of the width W.

εe is a little smaller compared to the substrate's dielectric constant εr since the fringing fields from the patch to the ground plane are not confined in only the dielectric however they are spread in the air as well. For the purpose of enhancing fringing fields from the patch, that cause radiation, the patch's width W will be increased. The increase of substrate thickness h and the reduction of εr will enhance the fringing fields. Substrates with thicker h and lower εr and microstrip patches with larger widths are used by MSA [36].

MSA are essentially narrowband. The standard MSA bandwidth is about 4-7 percent. A significant number of studies were carried out for the purpose of developing MSA. For increasing the impedance bandwidth, the methods employed are basically variations of 3 methods [37]:

- Increasing the volume of antenna via geometry alterations which focus of increasing the volume under patch (to increase thickness *h*), add more coupled resonators, decrease substrate dielectric constant.
- Application of matching network.
- Perturbing the geometry of antenna geometry for relocating or creating resonances through the use of slots and shorts in antenna.

A lot of applications use MSAs because of their advantages. The communication and telemetry antennas on missiles must be conformal and thin and are they are usually MSAs. Small arrays of microstrip radiators are used by radar altimeters. Additional aircraft-associated applications such as satellite communication and antennas for the telephone. The systems of satellite imaging use microstrip arrays. The patch antennas were applied on links of communication between satellites and ships or buoys. Because of their thin profile, MSAs are used by the systems of smart weapons systems. GPS, GSM, wearable devices, and pagers are the main users of MSA [36].

3.2.1 OVERVIEW TO MICROSTRIP PATCH ANTENNA

In its simplest form, micro-strip patch antennas, have radiating patch on a side of dielectric substrate that has a ground plane on the other side as displayed in the Figure 3.1. Mostly, a patch is composed of a conducting material like gold or copper and might take various shapes. Feed line and the radiating patch are typically etched or printed on dielectric substrate [38].

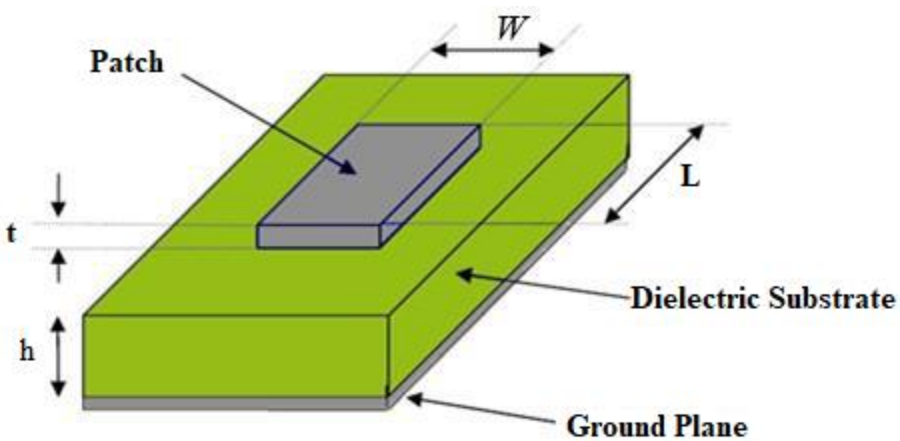

Figure 3.1: The basic structure of a microstrip patch antenna [38].

For rectangular patch, the patch's width W is usually $0.3333\lambda_o < W < 0.5\ \lambda_o$, here λ_o can be defined as the free-space wave length. The patch is selected extremely thin in a manner that $t << \lambda_o$ (t can be defined as the thickness of the patch). The dielectric substrate's height h is typically $0.003\ \lambda_o \leq h \leq 0.05\ \lambda_o$. The substrate's dielectric constant (ε_r) is usually in the range $2.2 \leq \varepsilon_r \leq 16$. [39].

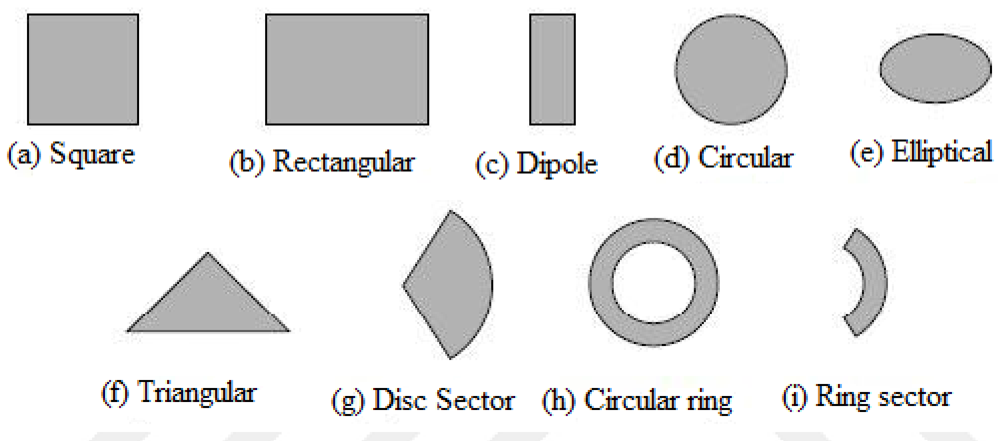

Figure 3.2: Types of patch antenna elements [39].

Micro-strip patch antenna radiates mainly due to the fringing fields between ground plane and patch edge. For optimum performance of antennas, it is desired having thick dielectric substrate with low dielectric constant due to the fact that this offers better effectiveness, optimum radiation and more bandwidth. Nevertheless, larger size antennas will be the result of these configurations. For the purpose of designing compact Micro-strip patch antennas, higher dielectric constants should be deployed that are less effective and lead to smaller bandwidth. Therefore, cooperation should be achieved between the performance and dimensions of antennas [36].

Microstrip antennas which are also known as patch antennas have become common because they provide the major benefit in that they provide the possibility that they can be printed on a circuit board directly [40]. The microstrip patch antenna is designed in such a fashion that it has two sides one which is the radiating side while the other is the grounded side. The radiating side has a patch that is made of gold or copper, and it can be designed into any shape depending on preference (rectangular, circular, and other shapes).

Modern technology enables the patch antennas to be used widely in the mobile market especially because they can be obtained at a low cost, can be fabricated easily and also their profile is low [41]. Their functioning is highly effective because they are made of high conductivity metal usually copper which is used in making the ground plane and the transmission line. The size of the microstrip patch antenna is represented by dimensions L, W and H whereby *L* represents the length, *W* is the width and H is the height. The height represents the thickness of the circuit board on which the microstrip is placed. The dielectric board has a certain measure of permittivity (ε_r) [41]. Although the thickness of the circuit board is important, it should be noted that the thickness should always be smaller than the operational wavelength. Usually, the height should be $1/40^{th}$ of the wavelength which is 0.025λ when expressed as a fraction. If the value is greater than that, then the efficiency of the microstrip becomes downgraded. To determine the frequency that the patch antenna will operate with, it is important to adjust the length of the antenna, and the following Equation can be used [41].

$$f = \frac{c}{\lambda} \tag{3.1}$$

Where f frequency, c speed of light, λ wavelength

$$f_r \approx \frac{C}{2L\sqrt{\varepsilon_r}} = \frac{C}{2L\sqrt{\varepsilon_0 \varepsilon_r \mu_0}} \tag{3.2}$$

From Equation 3.2, it is possible to deduce that it is a requirement that the wavelength should be twice as much as the length of the antenna or the latter should be half as much as the former when they are placed in the dielectric circuit board. While the length determines the frequency, the width is responsible for controlling the input impedance. It implies that adjusting the width so that it is large, the effect is that the resulting bandwidth. When Equation one is used and a square patch antenna is inputted, the input impedance that will be obtained is 300 Ohms. If the width is increased, then the impedance can be reduced, but it would require a very wide patch so that an input impedance of 50 Ohms can be achieved. This may not be practical because it leads to the consumption of a lot of space which may be valuable. The other aspect that is considered when dealing with the width, is the radiation pattern [42]. In order to calculate the radiation pattern after normalization, the following equations can be used.

$$E_\theta = \frac{\sin(\frac{k_W \sin\theta \sin\emptyset}{2})}{\frac{k_W \sin\theta \sin\emptyset}{2}} \cos\left(\frac{k_L}{2}\sin\theta\cos\emptyset\right)\cos\emptyset \quad (3.3)$$

$$E_\theta = \frac{\sin(\frac{k_W \sin\theta \sin\emptyset}{2})}{\frac{k_W \sin\theta \sin\emptyset}{2}} \cos\left(\frac{k_L}{2}\sin\theta\cos\emptyset\right)\cos\theta\sin\emptyset \quad (3.4)$$

Whereby the wavenumber (k) is calculated using Equation 3.5

$$k=\frac{2\pi}{\lambda} \quad (3.5)$$

And the field magnitude can be calculated using Equation 3.6

$$f(\theta,\emptyset) = \sqrt{E_\theta^2 + E_\emptyset^2} \quad (3.6)$$

3.3. FEEDING METHODS OF PATCH ANTENNA

At the end of designing, the feeding of the microstrip patch antenna (MSPA) is done. The main reason for this, it becomes possible to achieve high impedance for the input value by adjusting the dimensions of the feed. However, it is still possible to do a modification to the antenna so that better results can be obtained. Microstrip patch antenna has various methods for feeding.

These feeding techniques are often classified into 2 groups, non-contacting and contacting [41]. In the contacting group, the power is fed the patch directly by employing a metallic element. In the non-contacting group, the electromagnetic field is coupling with the patch.

The most three famous feed techniques that used to feed microstrip patch antenna (MSPA) are the coupling technique, coaxial probe, and microstrip line. The following subsections will discuss various techniques for feeding the patch antenna.

3.3.1 Microstrip Line Feed Technique

In this technique, a strip line is connected to the edge of the patch as shown in Figure 3.3 and Figure 3.4. The width of the patch is larger as compared to the width of the strip line. This technique has some advantages, where it is simple in modeling and ease of fabrication. This technique has two types; inset feed and Quarter-Wavelength Transmission Line feed. These types are discussed in the following subsections.

The summary of benefits and limitations are:

- Ease of fabrication,
- Simple to model,
- Impedance matching.

The limitations are:

- Feed radiation,
- Thicker substrate results in increasing the surface waves which limit bandwidth of the antenna.

3.3.1.1. Inset feed

As noted earlier, the current is found to be low at the ends of the patch antenna. As the distance decreases towards the mid-section, the current increases in magnitude. Therefore, it implies that it is possible to minimize the input impedance if the current is fed closest to the center. This can be achieved by including an inset feed that is shown in Figure 3.3 [43].

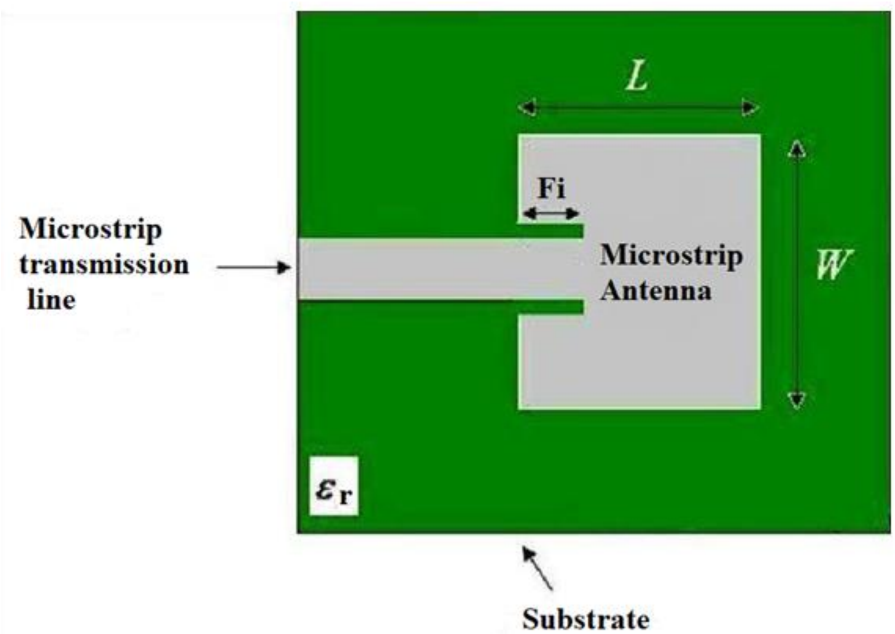

Figure 3.3: Inset feed indicated by R [39]

The current is found to have a sinusoidal distribution which implies that if the distance is increased further away from the end, then the current will be increased.

Notably, the voltage also experiences an increase by the same magnitude. The relationship between these parameters is represented by Z=V/I while the scaling of the impedance is represented by the Equation 3.7

$$Z_{in}(R) = cos^2\left(\frac{\pi R}{L}\right) Z_{in}(0) \tag{3.7}$$

3.3.1.2. Quarter-wavelength transmission line feeding

A Quarter-Wavelength Transmission Line of characteristic Z1 can also be used to match the Z_o represented in Equation 3.8. The matching is indicated in the Figure 3.4.

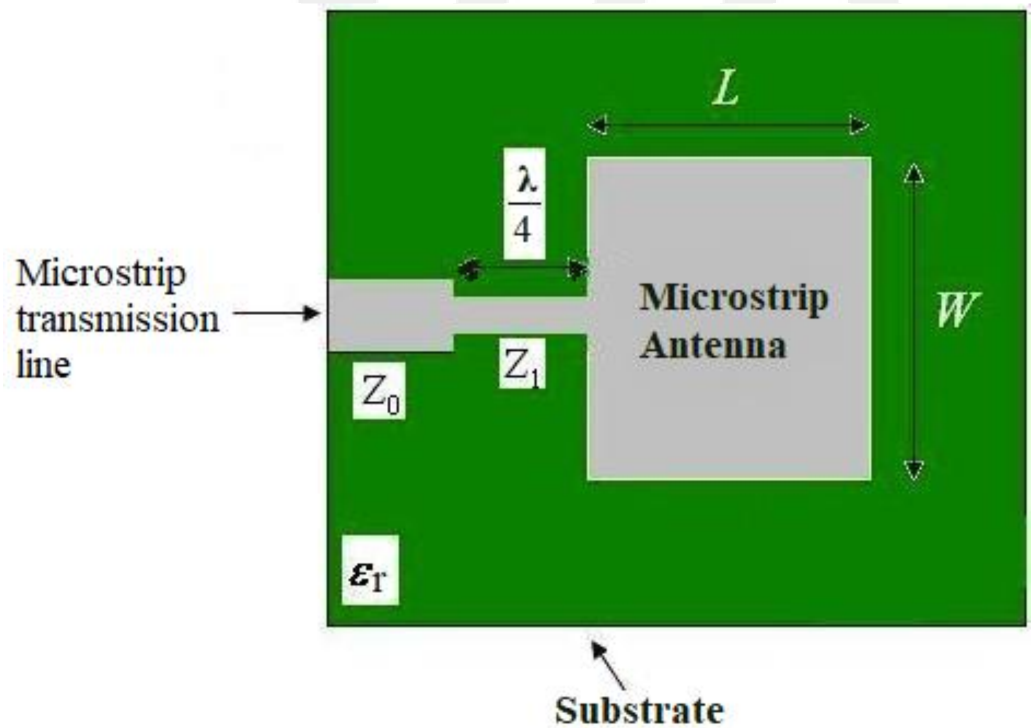

Figure 3 .4: Quarter wavelength matching [39]

In this scenario, three parameters are considered namely transmission line, input impedance, and the antennas impedance. The relationship is indicated in Equation 3.8.

$$z_{in} = z_0 = \frac{z_A^2}{z_A} \qquad (3.8)$$

Whereby (Z_{in}) represent input impedance, (Z_0) represents transmission line; (Z_A) represents impedance of the antenna, and (Z_1) represents variant impedance.

The objective in this scenario is to manipulate the values so that matching is achieved between the transmission line and the input impedance [41]. In order to cause variation that will result in matching, the variant impedance is altered so that the desired results are obtained. To alter the variant impedance, the quarter-wavelength strip‘s width is changed. As the strip is getting wider, the impedance Z0 will get lower and vice versa.

3.3.2. Coaxial Probe

This technique is very famous for feeding the patch antenna. It is also possible to feed a microstrip antenna using a probe so that the feeding process takes place from underneath. In this method, the outer conductor connected to the ground plane. While, there is an extension of the center conductor, which it goes up to the patch [43]. To control the impedance, adjust the position of the coaxial probe, and this is considered as an advantage of this method. However, it has some disadvantages like the bandwidth is narrow and making the antenna more inductive when the substrate height is increased, this lead to matching problems. It is also important to note that radiation in unwanted directions will take place because even the probe will radiate if height increases exceedingly. The summary of benefits and limitations are:

- Ease of fabrication,
- Ease of matching,
- Low level of false radiation.

The limitations are:

- Narrow bandwidth,
- Difficulty of model especially for thick substrate since a hole has to be drilled in the substrate,

With increasing substrate thickness, the input impedance becomes more inductive which leads to a matching problem.

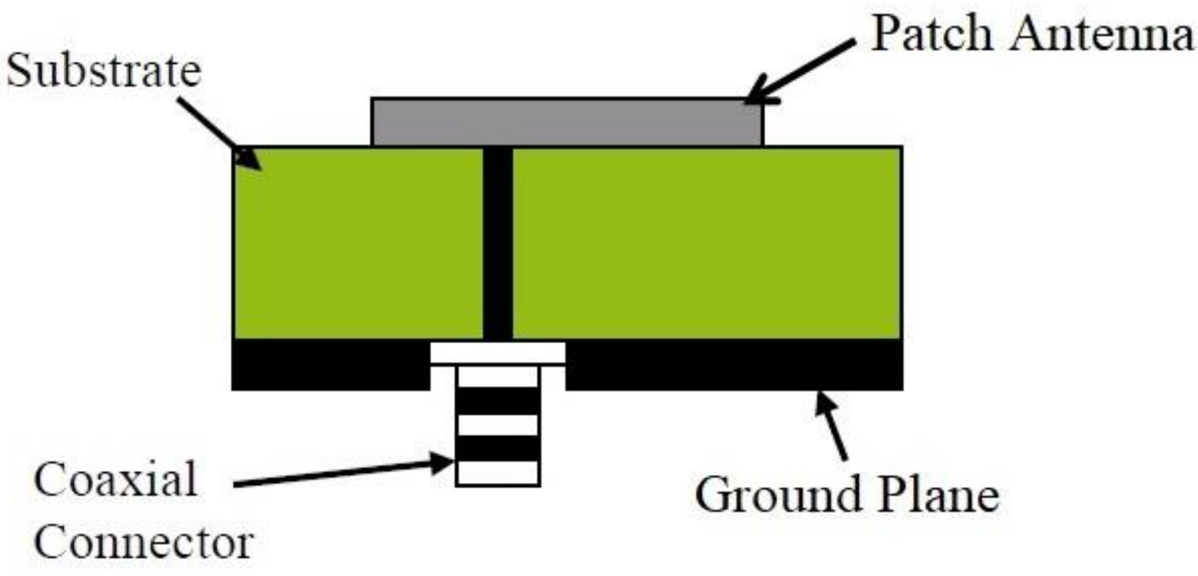

Figure 3.5: Probe feeding [43]

3.3.3. Coupled Feeds

The feeding method discussed in the previous section has some disadvantages regarding the width requirement in the microstrip antenna. For this reason, it is necessary to consider non-contacting feed techniques which have the capability of mitigating the negative implications of using these techniques [39]. The proximity coupled feeds and the aperture feeds are examples of the coupled feeds that are non-contacting techniques.

3.3.3.1. Proximity coupled feed

When using this technique, the patch antenna is designed in such a way that it has two dielectric substrates whereby the feed-line is located between the two substrates. In the case of the radiating patch, it is placed on top of the upper substrates surface [43]. Where there is a microstrip patch antenna that has radiating properties, the feed-line to the patch antenna is usually on the top surface of the two dielectric substrates. This feeding technique is preferred to other techniques because it offers many benefits. Some of these benefits include: it does not require any physical contact whatsoever between the element and the radiating surface. Another benefit of the proximity coupled method is that there is no drilling that is required and there is minimal spurring during emission of the radiation.

This method is efficient because it enables to achieve high levels of radiation which is brought about by the increased width of the patch.

The technique enables increasing the bandwidth by up to 13%. Using the proximity coupled feed technique enables optimization of the performance of the substrates. It makes it possible to optimize the performance of the feed technique separately from the performance of the patch. Although the technique has many advantages, two main advantages are associated with the technique. Also, the use of two different substrate layers increases the width of the patch.

The summary of benefits and limitations are:

- Elimination of false feed radiation,
- Providing very high bandwidth (as high as 13%),
- Matching can be done easily by regulating the length of the feed line and the width-to-line ratio of the patch.

The limitations are:

- Difficulty of fabrication due to the two dielectric layers which require proper alignment,
- Increase in the overall thickness of the antenna.

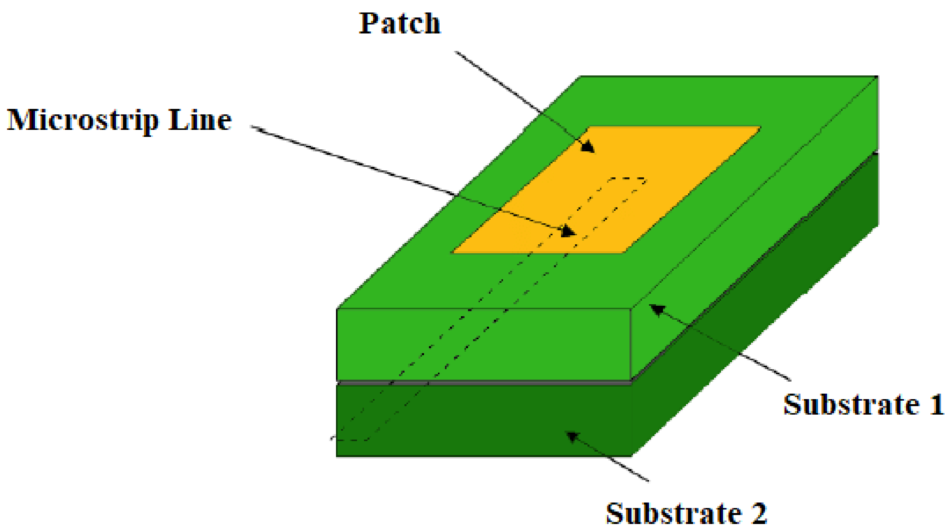

Figure 3 .6: Proximity coupled feed [43]

3.3.3.2. Aperture coupled feeds

Similar to the proximity coupled technique, the aperture method also uses electromagnetic coupling technology. This technique involves having a common aperture that is utilized in coupling the RF energy that is radiated from the microstrip patch antenna [39]. The common aperture is placed on the ground plane whereby there may be one or more conducting patches according to the desired performance expected. A layer of dielectric carrier supports the patches on the ground plane. To increase the efficiency of the microstrip patch antenna, the coupling aperture is situated at the central part of the patch. Variations in a number of factors dictate the magnitude of coupling that is derived from the feed line. The factors are such as; location, shape and size of the aperture that is placed in the central part of the microstrip patch antenna. The location of the radiating patch element is at the top of the feed substrate, and the ground plane is placed between the two substrates. The ground plane between the two substrates has the coupling slot. This design where the ground plane is placed between the substrates enables minimizing the spurious radiation. Aperture-Coupled feeding has a number of other advantages. The other benefits include; ease of integration and the amount of space available becomes increased.

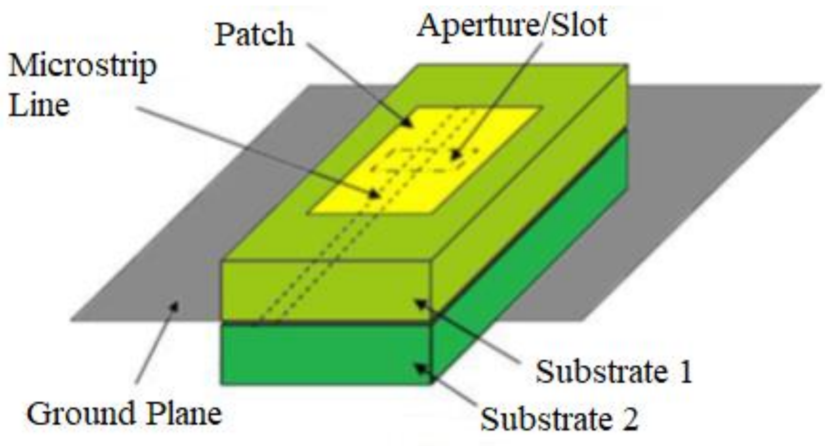

Figure 3 .7: Aperture feed technique [39]

Optimal antenna performance can be achieved because it is possible to do an independent selection of the feed substrates and the radiator.

A higher dielectric constant can be chosen to ensure that the electrical size of the circuit is reduced. To ensure that the dielectric constants of the two substrates have an effect on each other, the ground plane is introduced.

The aperture feed technique is advantageous in the following way; it leads to an increased degree of freedom which allows for optimization of the design. The process of matching the impedance becomes easy for designers because there is an additional degree of freedom [39].

For matching purposes, adjusting the length of the open-circuit stub adjusts the antenna‘s locus which enables compensation of the reactance.

The advantages are:

- False radiation is minimized since the ground plane separates the patch and the feed line.

The Limitations are:

- The difficulty of manufacturing due to the presence of multiple layers, which increases the thickness of the antenna.

- Narrow bandwidth.

In summary, Table 3.1 presents a comparative demonstration of the previously described feeding techniques.

Table 3.1: Comparison among the various feeding methods [36], [37].

Properties	Aperture Coupled Feed	Proximity Coupled Feed	Microstrip Line Feed	Coaxial Feed
Spurious Feed Radiation	Less	Lowest	High	High
Reliability	Decent	Decent	Better	Bad because of soldering
Simplicity of Fabrication	Alignment needed	Alignment needed	Simple	Drilling and soldering is required
Impedance Matching	Simple	Simple	Simple	Simple
Bandwidth (accomplished with impedance matching)	2-5 %	13 %	2-5 %	2-5 %

3.4. ANTENNA CHARACTERISTICS

There are too many important parameters in order to define the characteristics of antenna, such as directivity, return loss, radiation pattern, gain, polarization, antenna efficiency, input impedance and others which are well defined in the literatures [37], [38], [40], [41]. However, in order to satisfy the content of this thesis, some important parameters will be explained.

3.4.1. Radiation Pattern

The main and major characteristic of the antenna is the radiation pattern. As it is an important characteristic of the antenna, it can be defined as the graphical representation of the properties of radiation of the antenna. The antenna is graphically surrounded by the sphere which is evaluated by the electromagnetic fields at the same equivalent measure of distance to the radius of the sphere [37], [41]. The radiation pattern, being a graphical representation of the properties of radiation of an antenna, it represents the antenna in three dimensions; three graphical dimensions. They represent the antenna in three dimensions being as a function of the angular direction. The E-plane of the patch antenna is the plane that has in it the field vector. On the other hand, H-plane is the plane that has the H-vector in it. The appropriate angle of the dipole where the H-plane is concerned is 90 degrees.

The omnidirectional antenna pattern is known as the type of the antenna pattern that is demonstrated where there is no kind of variation that is seen from the radiated E/H fields. The antenna pattern is most of the times plotted in the dB. Superfine features of the antenna pattern can be obtained when using a logarithmic scale when plotting. The patch antenna has a pattern that is a recurring pattern, where many of the base patch antennas have the major lobe and then the minor lobes which are also referred to as the side lobes. The back lobe is a side lobe which is occurring on the immediate opposite direction of the main major lobe. There are four major patch antenna pattern types that are;

- Omnidirectional antenna pattern type. This is an antenna pattern type where the response to the radiation is always constant in only one of the principal planes of the patch antenna.
- Isotropic antenna pattern type. This is an antenna pattern type where the patch antenna radiates gives out radiation in all directions in equal and the same measure in the 3D space. This is used to prove how the patch antennas are directive even though it is impossible to prove it in a theoretical manner.
- Broadside antenna pattern type. This is an antenna pattern type where the major and the main beam of the antenna are usually normal to the axis or to the plane that has the antenna.

- End-fire antenna pattern type. This is an antenna pattern type where the main and major beam of the antenna is usually contained in the plane or is parallel to the plane that is containing the patch antenna.

3.4.2. Directivity

The directivity is the measure of the quantity of the concentration given off by the antenna in a certain given direction. There has to be known antenna for the directivity of the antenna to be measured, and the known antenna is always an isotropic radiator. In technical terms, the directivity of an antenna is a function of a specific angle that can be plotted in either 2D or a 3D plot. The directivity of the antenna also shows the representation of the power which is added and that is collected in a given specific direction that equals an isotropic radiator. The additional power that is collected or transmitted does not come from nothingness. The additional power comes from the directivity in the other directions. The patch antenna has more products geared towards one specific direction where there are other responses in other directions. The extra additional power is obtained at the expense of the directivity in other directions. Usually, the patch antenna‘s directivity is estimated at a value ranging from 2 to 7 dB, and they are placed horizontally when viewing the microstrip and at the same time it is found that the linear polarization is evidenced in the fields when the radiation pattern is normalized [37].

3.4.3. Gain

The gain denotes what proportion power is transmitted within a certain direction to the power that transmitted of an isotropic source in the same direction. The gain is used commonly more than the directivity because it takes under consideration the particular losses that occur. If the gain of an antenna is three dB, this implies that the power that received far away from the antenna is going to be twice as much as what would be received from a lossless isotropic antenna with the identical input power [41]. The gain is related to the efficiency of the antenna and the directivity by Equation 3.9:

$$D = \varepsilon_{RG} \tag{3.9}$$

Except for dB, there are other units for antenna gain, those are:

- dBi: describes the gain relative to an isotropic antenna.

- dBd: describes the gain relative to a dipole antenna.

3.4.4. Antenna Impedance

The antenna input impedance is a key concept to put under consideration for the system RF will have to interface to the antenna. It is disadvantageous for the impedance of the antenna to be unmatched to the system [38]. This is because when the impedance is mismatched; there will be a lack of proper transmission of power to and from the antenna. The improper transmission of power is brought at the reflection produced when the impedance is not matched.

3.4.5. Surface Current

The surface current is an actual electric current that is induced by an applied electromagnetic field. The electric field pushes charges around. The patch antenna has an open-end circuit that makes the current at its end equal to 0. While, the current is maximum at the center of the patch antenna; therefore, this makes the current zero at the farthest ends. It shows the amount of the impedance on the surface [37].

3.4.6. Gain or Directivity in dB

The dB units are the most appropriate units to express any changes in magnitude orders. The dB units give room for the calculations in multiplications and divisions to be replaced by simple addition and subtraction calculations. This is seen in the case of radio systems where the dB units are used to express quantities since the quantities are subject to a variance of many magnitude orders. There is always a reference where a dB quantity is involved. In the case of directivity where the patch antenna is involved, the average intensity of radiation that is transmitted by the isotropic radiator is the denominator which in turn is the reference. From the previous statement, it can be observed that directivity is usually the comparison of the microstrip patch antennas. An isotropic radiator is a reference when finding the directivity of the patch antenna. An isotropic radiator becomes the reference by replacing the dB with the unit dBi. The dBi units are used when there is another reference that is used apart from an isotropic radiator [41].

3.5 MICROSTRIP RESONATORS

In this segment, different sorts of microstrip resonators are displayed and examined. The foremost commonly utilized resonators are: stepped-impedance resonator (SIR), ring resonator, meander-loop resonator, and substrate-integrated waveguide resonator (SIW).

3.5.1 Stepped-Impedance Resonator (SIR):

The structure of the SIR is appeared in Figure 3.8. The SIR could be a non-uniform transmission line comprises of two areas, high-impedance and low-impedance segments.

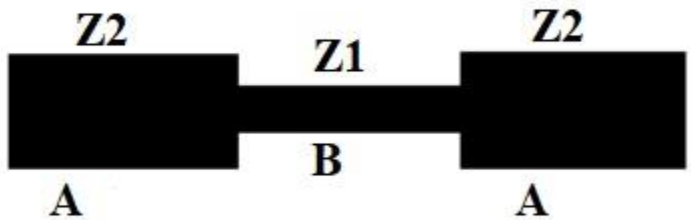

Figure 3.8: Schematic of the Stepped-impedance resonator [45].

The characteristic impedances for each line area are signified as Z_1 and Z_2 with electrical lengths A and B separately [3]. The input induction can communicate by [44]:

$$Y_{in} = \frac{2jY_2(KK_1+K_2)(K-K_1K_2)}{K(1-K_1^2)(1-K_2^2)-2(1-K^2)K_1K_2} \qquad (3.10)$$

Where $K_1 = \tan\left(\frac{A}{2}\right), K_2 = \tan(B)$ and $K = \frac{Z_2}{Z_1}$. The SIR is used for the structures that require wide rejection bands [45].

3.5.2 Square-Loop Ring Resonator

Figure 3.9 shows up the structure of the square-loop ring resonator. The resonator comprises four undefined sides related to making a square closed circle and two coupling gaps [46].

In case one of the coupling gaps has been opened, the effect of the ring resonator on the resonation repeat will be less and inclusion coupled will be decreased. There's another way to amplify the coupling and diminish the consider loop current is to shield the ring resonator with a dielectric or utilizing restricted copper tape over the cleft [47].

3.5.3 Meandered Resonator

In figure 3.10, a 2-D meandered resonator is displayed which has the same length and measurements of the 2-D Hilbert resonator, this implies that the capacitance are break even with for each setup. So, on the off chance that the inductances are not rise to this implies that the resounding frequencies will be diverse for each structure.

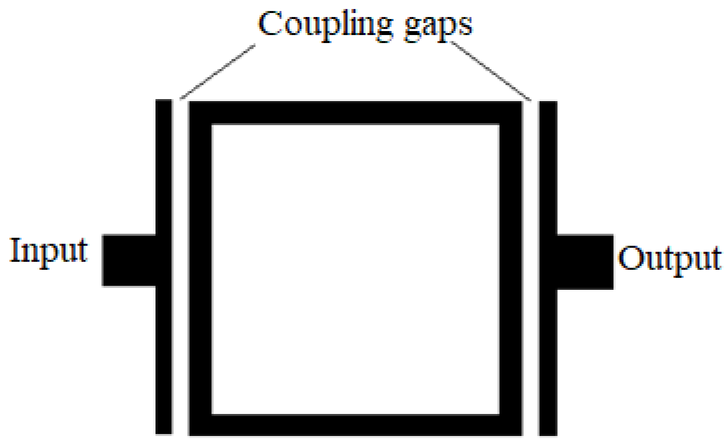

Figure 3.9: General structure of the square-loop ring resonator.

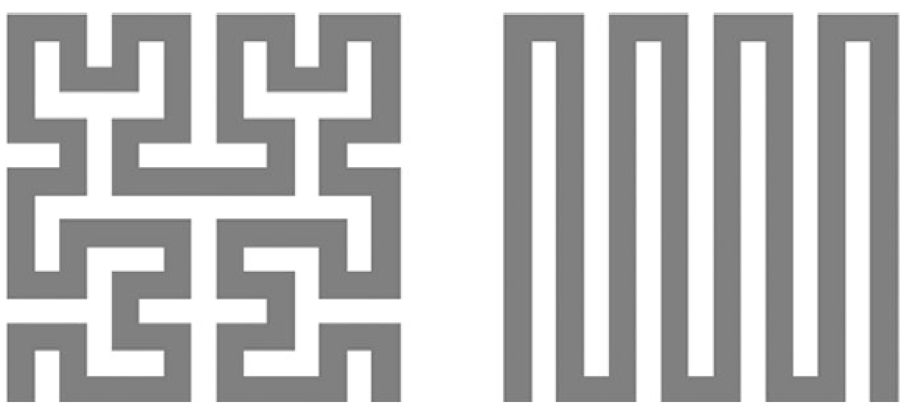

Figure 3.10: 2-D meandered and 2-D Hilbert microstrip resonators with the same length and spacing [48].

The total inductance per length of the meander, L_{tot} is given by [48]:

$$L_{tot} = 2nL \tag{3.11}$$

Where n is the number of meander turns, and L represents the inductance per length for each straight line segment.

3.5.4 Substrate-Integrated Waveguide (SIW) Resonator

The demand for using this type of resonator has increased in recent years due to its low cost, compact, good measurement, and great integration with circuits and other waveguides for coupling and achieving acceptable results. Figure 3.11 shows the SIW area, a rectangular waveguide with metal slot air holes attached from the top layer to the ground layer of the waveguide. S_a is the division between discussion gaps and D_a is the width of each gap, while S_v is the division between two adjacent minerals through sans D (v) is the distance across each through.

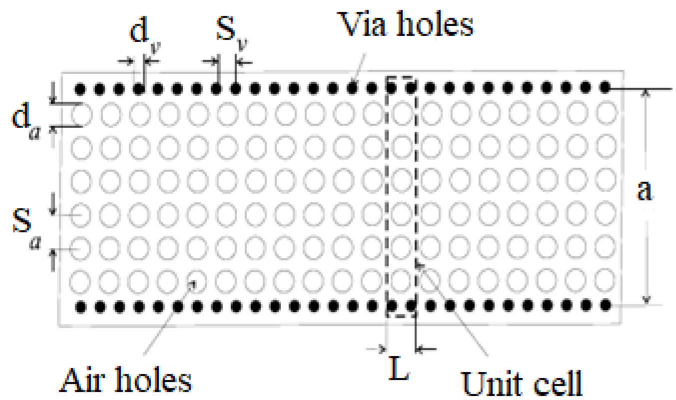

Figure 3.11: Scheme of SIW with air holes and metallic vias [49].

The SIW can be considered as a rectangular wave-guide to calculate its effective width a_{eff} by [49]:

$$a_{eff} = a - \frac{d_v^2}{0.95 S_v} \tag{3.12}$$

The concept behind the metallic via is to carry more signals from input to output ports, hence reducing radiation losses and achieve size miniaturization.

3.6 COUPLING TYPE FOR TRANSMISSION LINES

There are various ways for coupling of microstrip Microwave resonators, and each method gives different resonances. Figure 3.12 shows the three types of coupling, namely: electrical coupling, magnetic coupling, and mixed coupling [50].

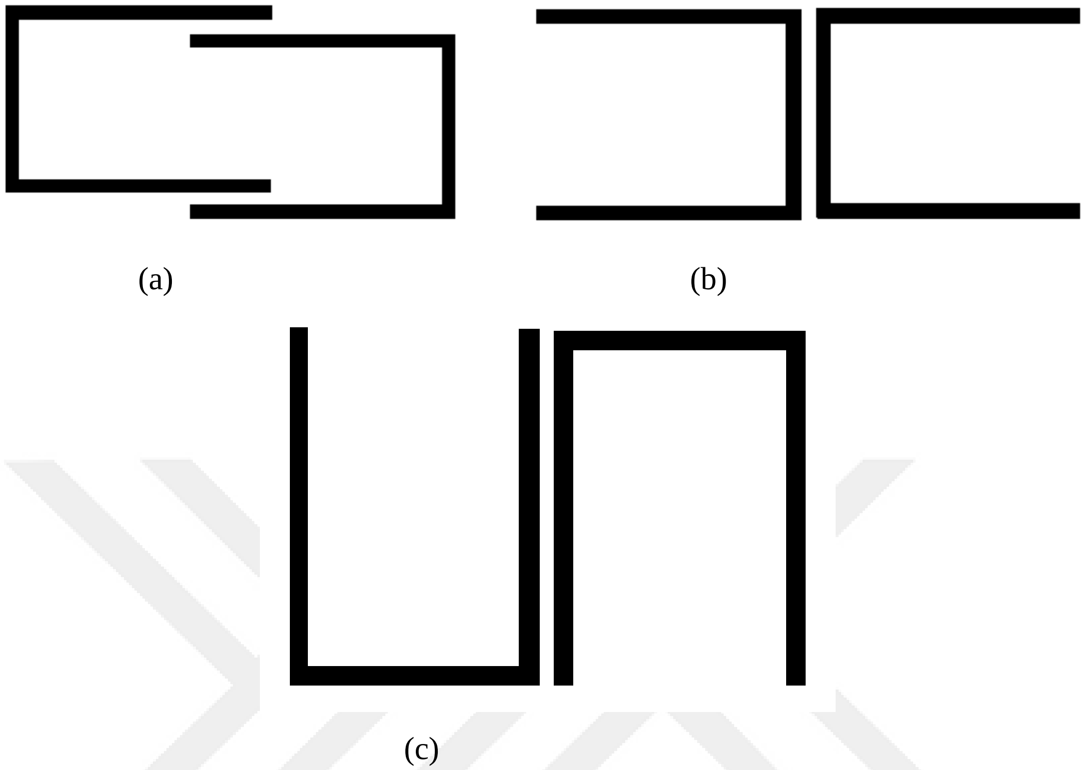

Figure 3.12: Transmission lines coupling schemes: (a) electric; (b) magnetic; (c) mixed.

3.6.1 Electric Coupling

The lumped element for the electric coupling structure of Figure 3.12(a) is shown in Figure 3.13 (a), where L and C are inherent conductor inductor and capacitor, to realize from $1/\sqrt{LC}$ the resonant frequency of the resonator, and C_m denotes the mutual capacitance. The equivalent circuit of Figure 3.13(a) can alternated to the circuit represented in Figure 3.13 (b) [50].

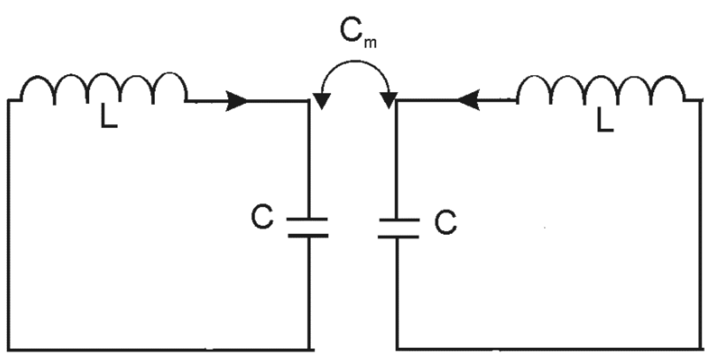

(a)

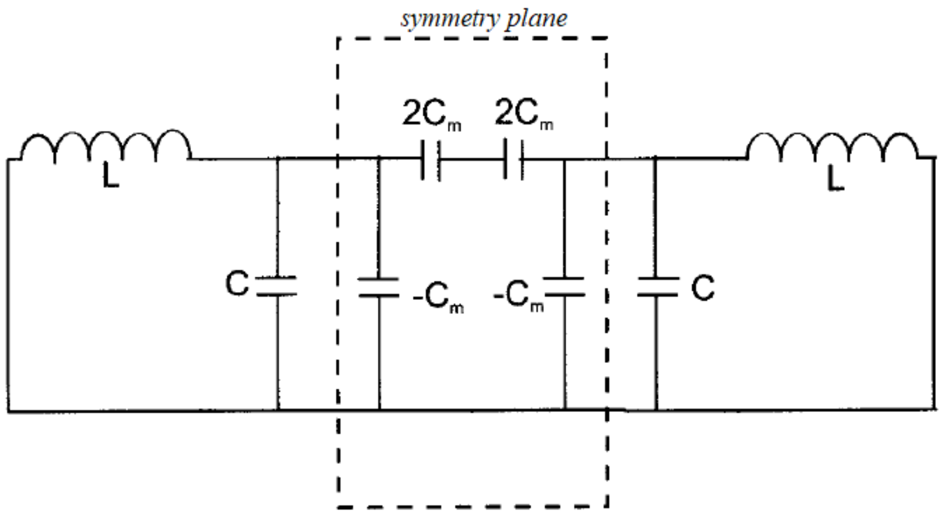

(b)

Figure 3.13: Electric coupling: (a) lumped equivalent element; (b) alternative form of an equivalent circuit [50].

The symmetry plane of Figure 3.13(b) is replaced by a short circuit (electric wall), so the resonance frequency is given by [50]:

$$f_e = \frac{1}{2\pi\sqrt{L(C+C_m)}} \tag{3.13}$$

This recurrence is lower than that of the uncoupled single resonator due to the coupling impact which upgrades the capacity for charge capacity for the single resonator when the electric divider is embedded into the symmetrical plane of the coupled resonator. Presently, supplanting the symmetry plane of Figure 3.13(b) by an open circuit (significant divider), the reverberation of the circuit will be:

$$f_m = \frac{1}{2\pi\sqrt{L(C-C_m)}} \tag{3.14}$$

In the event that the recurrence expanded, the coupling impact diminishes the capacity to store charge. We can be utilized to extricate the electric coupling coefficient k_E [50]:

$$k_E = \frac{f_m^2 - f_e^2}{f_m^2 + f_e^2} = \frac{C_m}{C} \tag{3.15}$$

2.6.2 Magnetic Coupling

The lumped component for the coupled resonator of Figure 3.12(b) is appeared in Figure 3.14(a), where L_m indicates the shared inductance. The coupling between the two resonator circles by an impedance inverter. Figure 3.14(a) can be rotated to an identical circuit that appeared in Figure 3.14(b) [1, 21]. On the off chance that the symmetry plane of Figure 3.14(b) is supplanted by a brief circuit (electric divider), the recurrence can be given by [52]:

$$f_e = \frac{1}{2\pi\sqrt{(L-L_m)C}} \tag{3.16}$$

When the electric divider is embedded within the symmetrical plane, the resounding recurrence expanded due to the coupling impact reducing the put away flux within the single resonator circuit.

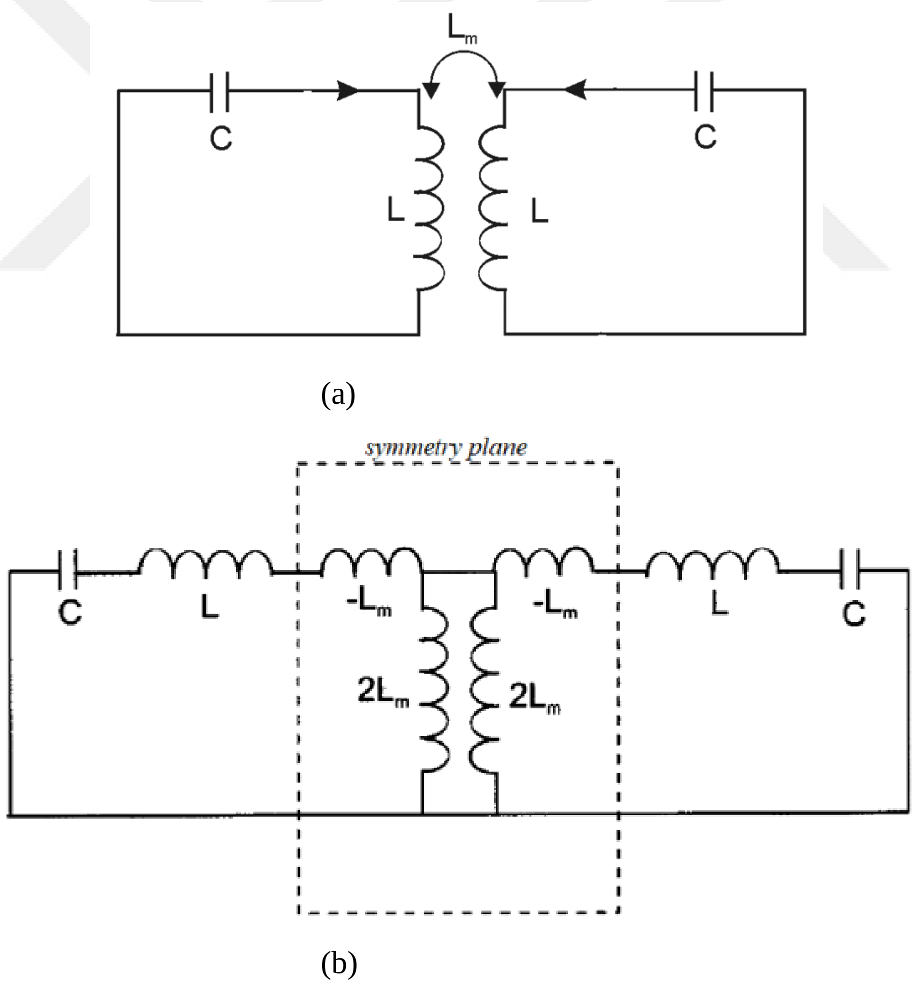

Figure 3.14: Magnetic coupling: (a) lumped equivalent element; (b) alternative form of an equivalent circuit [52].

Within the case of embedding an open circuit (significant divider) rather than the symmetrical plane, the resonance recurrence is:

$$f_m = \frac{1}{2\pi\sqrt{(L+L_m)C}} \quad (3.17)$$

It is apparent that the resonance is reduced due the coupling impact that increments the surface current flux. From conditions (3.14) and (3.15), the attractive coupling coefficient k_m can be found:

$$k_m = \frac{f_e^2 - f_m^2}{f_e^2 + f_m^2} = \frac{L_m}{L} \quad (3.18)$$

2.6.3 Mixed Coupling

Figure 3.15 shows the lumped element for the mixed coupled structure of Figure 3.12(c). Similarly, by inserting an electric wall and a magnetic wall one at a time instead of the symmetrical plane of Figure 3.15, the resonances can be obtained as shown [51]:

$$f_e = \frac{1}{2\pi\sqrt{(L-L'_m)(C-C'_m)}} \quad (3.19)$$

$$f_m = \frac{1}{2\pi\sqrt{(L+L'_m)(C+C'_m)}} \quad (3.20)$$

As can be seen, both the magnetic and electric couplings have the same effect on the resonant frequency shifting.

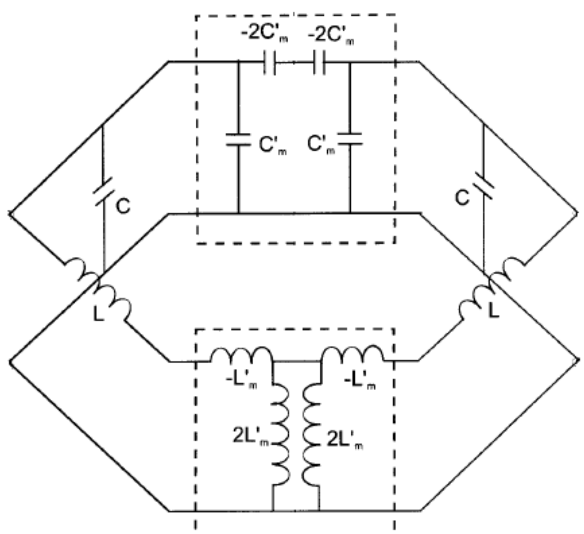

Figure 3.15: Mixed coupling lumped element [51].

By solving equations (3.17) and (3.18), the mixed coupling coefficient k_x is obtained:

$$k_x = \frac{CL'_m + LC'_m}{LC + L'_m C'_m} = \frac{f_e^2 - f_m^2}{f_e^2 + f_m^2} \tag{3.21}$$

4. APPLICATION OF FRACTAL GEOMETRY IN SLOT ANTENNA DESIGN

4.1 INTRODUCTION

In this chapter, the unique characteristics of fractal geometries will be presented together with the most commonly used fractal geometries applied in the slot antenna design. Regarding this subject, the application related to fractal geometries in slot antenna design could be grouped into two types. In the first category, the fractal geometry is applied directly such that it constitutes the whole slot structure, while in the second one; the fractal geometry is applied indirectly. In this case, there is a slot structure with Euclidean shape, such as triangle, square…etc., and fractal geometry has to replace each line segment in this structure.

4.2 FRACTAL PROPERTIES

Fractal indicates irregular or broken fragments; the term fractal has been initially presented through Mandelbrot [53] for describing a family of complex shapes which have non-integer dimension and have inherent self-similarity in their geometrical structures. Which is why, there is a necessity for a geometry which is capable of handling such complicated shapes more efficiently compared to the Euclidean geometry, which has dimensions of integer number, like 1-D line, or 2-D planes...and so on.

Many fields of engineering and science use fractal geometry [54]-[57]. A major area of fractal is its use in the antenna design for producing multiband and compact antennas taking advantage of their exceptional features such as self-similarity and space filling [58].

Fractal shaped antennas show certain promising properties, which are associated with their geometrical characteristics. Generally, the fractal structures are composed of multiple copies of themselves at various scales and the fractal's size is defined through the iteration number and the initiator. The fractal that is utilized in designing antennas is typically quasi-fractal or pre-fractal yet not mathematically fractal geometry with infinite scale. Thus, quasi- fractal of many iterations could be used for certain multi-band antennas. All frequency bands are conforming to a certain fractal's scale [59].

Fractal antenna engineering can be defined as a developing field which uses the concepts of fractal to develop novel antenna types with distinguished properties. The self-similarity related to fractal structures cause antenna' multiband behavior and frequency-selective surfaces. On the other hand, the space-filling properties lead to miniaturized and compact size antennas. Recently, extensive studies were focused on fractal antenna engineering. Fractal methods were utilized to loops, monopoles, patches, dipoles, and slot antennas [60]-[64].

4.2.1 Space-Filling

Fractal curves can be distinguished through a special feature that, following infinite iterations, their length become infinite even though the whole curve fit into finite area as shown in Figure (4.1). Such feature could be used for miniaturization of microstrip and printed antennas through increasing the effective electrical length via which current travels. Many applications can benefit from fractal antennas. The continuous development in the field of wireless communication has increased the necessity for compact integrated antennas. Space saving capabilities which are related to fractals to effectively fill a small amount of space provide special benefit of applying integrated fractal antennas over Euclidean geometry [65]

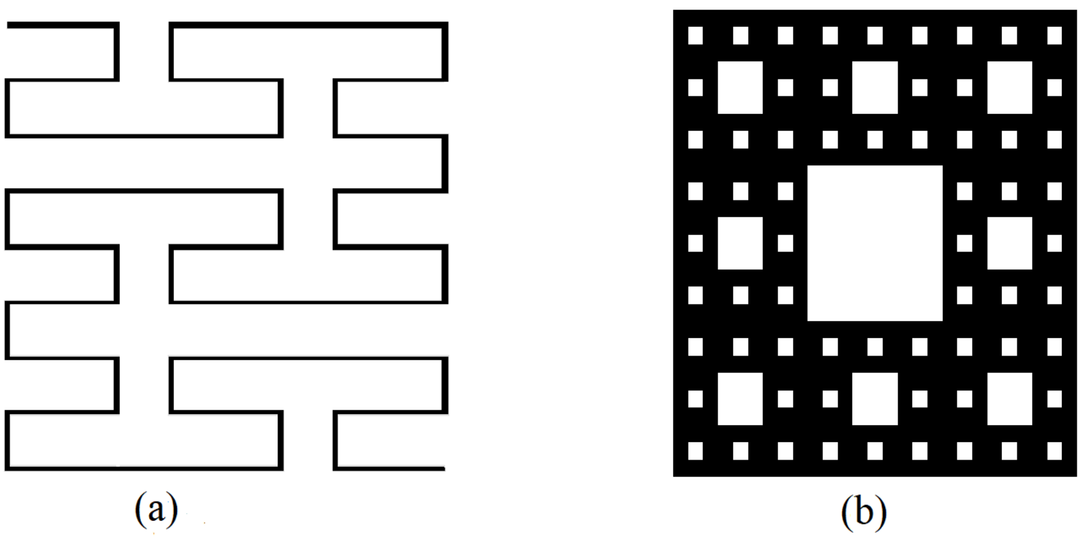

Figure 4.1: Space-filling fractals of (a) 3rd iteration Peano carpet, and (b) 3rd iteration Sierpinski carpet [66], [67].

4.2.2 Self-Similarity

Self-similarity property means that a small part of the structure is a scaled-down copy of the original structure, as displayed in Figure (4.2). Therefore, antennas can operate at multiple frequency bands. Traditional fractal geometries including Minkowski, Cantor, Koch, Sierpinski, Hilbert, and other fractal curves were efficiently utilized for producing multi and dual band printed slot antennas for many wireless applications [68].

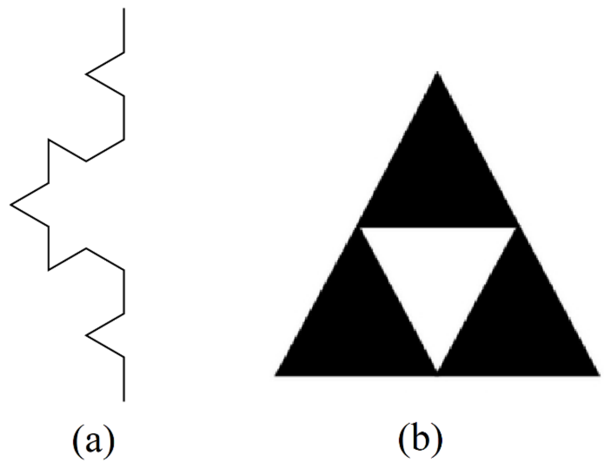

Figure 4.2: Self- similar fractals of (a) second iteration Koch curve, and (b) second iteration Sierpinski gasket [66], [67].

4.2.3 Fractal Dimension

The main feature of fractals is that they have non-integer dimensions dissimilar to the Euclidian which have integer dimensions. The common intuitive concept of dimension is called the topological dimension. A cube, line segment, point and a square, as displayed in Figure (4.3) have topological dimensions of 0, 1, 2 and 3, respectively. An integer number is always used for expressing the intuitive dimension [67].

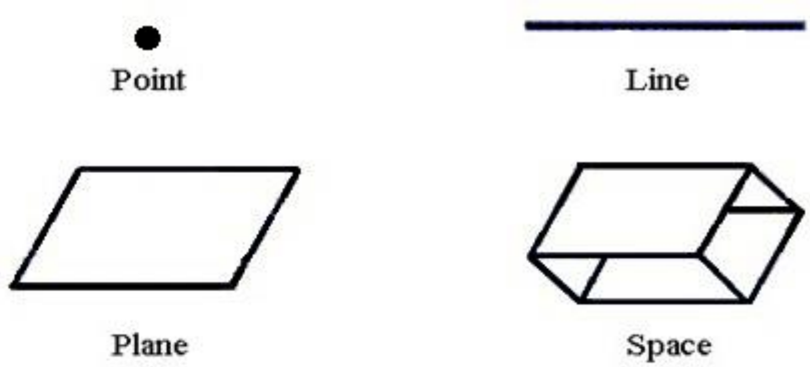

Figure 4.3: Euclidean geometries [67].

Fractal dimension is associated to the self-similarity in that the simplest method for creating a figure that has fractal dimension by self- similarity. Then, the fractal dimensions (FD) will be, as given by [65]:

$$FD = \frac{log_{10}(N)}{log_{10}(1/r)} \tag{4.1}$$

Where N can be defined as the overall number of distinct copies, r can be defined as the reduction factor value that indicates how will be the new side length regarding the original side length.

In order to calculate the fractal dimension of any self-similar shape, the shape can be split into N parts, where the size of each part is related to the size of the original one by the reduction factor value. The fractal dimension FD equals the topological dimension for any Euclidean shape, but FD can also be evaluated for any non-standard shapes that exhibit self-similarity [69].

Dimension of some geometrical shapes are listed below in Table (4.1). The fourth column contains the FD value for each shape, where FD is calculated using equation (4.1). Figure (4.4) demonstrates Euclidean geometrical shapes which are split into N parts by using a reduction factor of 1/2 to divide a line segment, square and cube [70], [67].

Table 4.1: Dimensions of geometrical shapes

Shape Name	***r***	**N**	**FD**
Line	½	2	1
Square	½	4	2
Cube	½	8	3
Cantor Set	1/3	2	0.63
Sierpinski Gasket	½	3	1.58
Minkowski Island	1/3	5	1.46

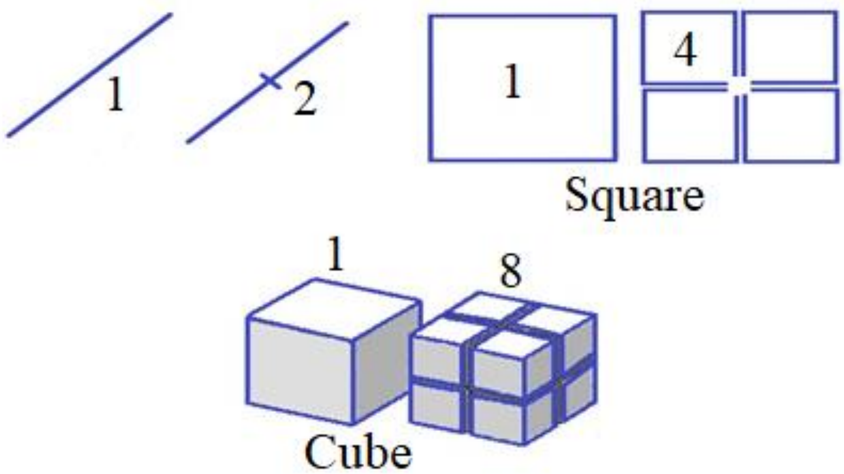

Figure 4.4: Euclidian geometrical shapes with a reduction [66], [67].

4.3 FEATURES AND LIMITATIONS OF FRACTAL GEOMETRIES IN ANTENNA DESIGN

Features:

- Miniaturization.
- More efficient input impedance matching multi and wide bands (utilizing single antenna rather than several).
- Decreased mutual coupling in the fractal array antennas
- Frequency independent (reliable operation throughout large ranges of frequency).

Limitations:

- Complexity (some types are complex to construct).
- Numerical limitations (become less with the continuing advance in computer technologies).
- The benefit begins to diminish after first few iterations.

However, the features offered by the fractal geometries are more than limitations that they have encountered. In addition, the advances in computer technologies and the computational techniques have contributed to make these limitations less important [70], [67].

4.4 COMMONLY USED FRACTAL GEOMETRIES IN ANTENNA DESIGN

Large number of fractal geometries and their variants are reported in the literatures [53], [65], [69], but very limited numbers among these were adopted in designing antennas for various applications.

In the following subsections, a presentation of the most commonly used fractal types.

4.4.1 Cantor Set

Cantor set can be defined as a standard fractal object that displays precise self-similarity through all scales [65].

Cantor set include infinite set related to the disappearing segments of the line in unit interval. The optimal way for understanding Cantor set fractal is displaying its construction approach, as shown in Figure (4.5) for the plainest type of Cantor set (the triadic Cantor set).

The set will be created via eliminating the middle third of unit line segment (step k = 1 in figure). From the two segments that remained of the line, every one of which is 1/3 in length, middle thirds will be removed once more (step k = 2 in the figure). Middle thirds of the 4 of the rest of line segments, every one of which is 1/9 in length, will afterwards be eliminated (k = 3) and similarly to infinity. The remaining is considered as a set of infinitely various disappearing segments of the line that lie on unit interval that's combined and individual lengths come close to 0. Such point set is referred to as Cantor dust or Cantor set [71].

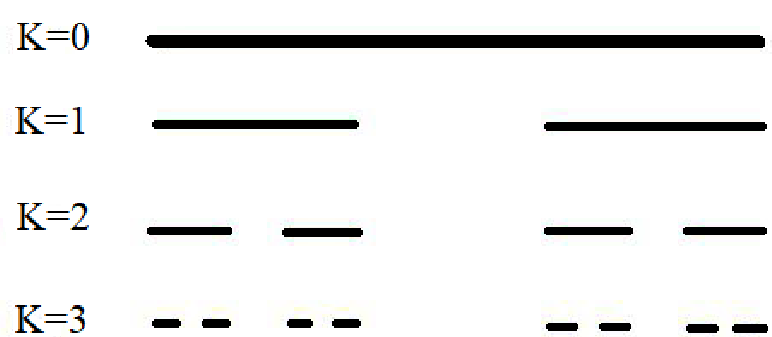

Figure 4.5: The generation of Cantor set [65], [67].

Regarding the Cantor set construction, the initial unit line segment k = 0, is referred to as the set's initiator. The initial stage, k = 1, is referred to as the generator or motif, since it is considered as the repeated iteration related to this stage on the following line segment that result in the set's creation. It is necessary repeating the generation procedure only via the number of stages needed to deceive the eye, and not countless times (which is considered accurate for every illustration that is related to fractal objects). Yet, the Cantor set is obtained following infinite number of iterations. A set of line segments with a particular measurable length are produced via a finite number of iterations. Such objects created *en route* to fractal object are referred to as pre-fractals [72], [73].

4.4.2 Koch Curve

This construction method is displayed in Figure (4.6), it is considered as an extra sufficiently documented fractal. Just like the Cantor set, Koch curve is easy to construct through the use of iterative process starting with set's initiator as the unit line segment (stage $k = 0$ in figure). The unit line segment will be separated to thirds, the middle one will be eliminated. After that, the middle third will be substituted by 2 equal parts, they two are 1/3 in length that create an equilateral triangle (stage $k = 1$): this stage is the curve generator. In the following stage ($k = 2$), the middle third will be eliminated from the 4 segments, every one of which will be substituted by 2 equal segments. Koch curve will be produced after repeating this procedure for an infinite number of times. Once more, the set's self-similarity is obvious: all sub-segments are considered as carbon copy of the original curve, as displayed in Fig. (4.6) [74].

A visible feature of Koch curve is that it apparently has an infinite length. Which could be visible from the process of construction. At every stage, k, in its generation, the length regarding the prefractal curve will increase to L_{k-1}, where L_{k-1} can be defined as the length of the curve in the previous stage.

It might be visible that Koch curve is efficiently produced from corners, thus, there is no unique tangent happens upon it. Koch curve isn't a smooth, also it is nowhere-differentiable, as unique tangent, or slope, cannot be found upon it. It is a fractal object that possesses a fractal dimension. Every one of the smaller segments of the Koch curve is a precise simulation of the entire curve [75].

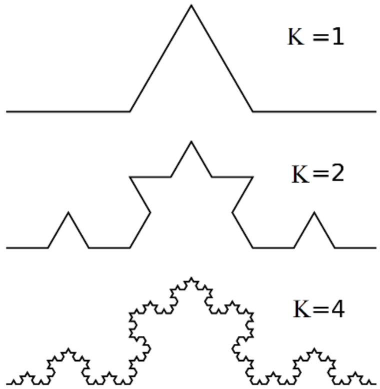

Figure 4.6: The generation of Koch curve [75].

4.4.3 Sierpinski Gasket and Carpet

The construction which is related to Sierpinski gasket is displayed in Fig. (4.7). Filled triangle in the plane is the initiator in such case. The middle triangular part will be eliminated from original triangle. After that, the central triangular segments will be eliminated from the rest of the triangular elements etc. Sierpinski gasket is created following an infinite number if iterations. All pre-fractal step in construction are composed of 3 smaller copies of the previous step, every one of the copies is scaled through a factor of 1/2 [76].

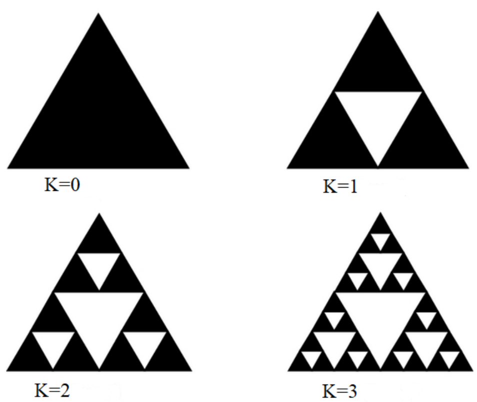

Figure 4.7: The generation of Sierpinski gasket [76].

Sierpinski carpet is another variant of Sierpinski gasket, it is displayed in Fig. (4.8). The construction approach for gasket and carpet are similar. In this case, the initiator is a square and the generator will remove the central square, that its side length 1/3 of the original square. With Sierpinski carpet and gasket, the constructions cause fractal curves whose area vanishes [77].

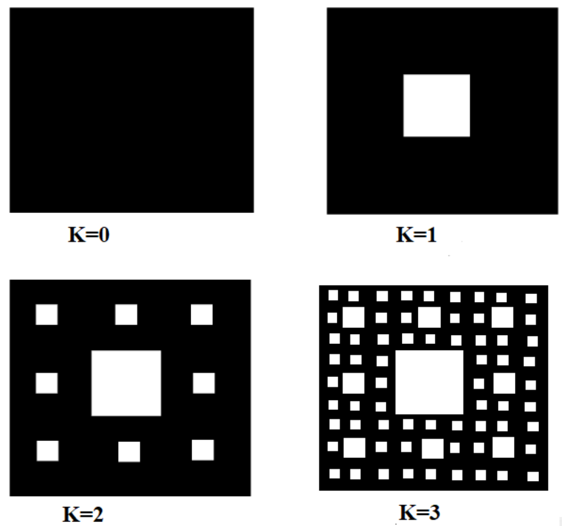

Figure 4.8: Generation of Sierpinski carpet [77].

4.4.4 Minkowski Island Fractal

The starting geometry regarding Minkowski island fractal, referred to as initiator, is a Euclidean square. All the 4 straight segments related to the starting structure will be substituted by generator, which has been displayed at the bottom of Fig. (4.9). This iterative generating process will continue for infinite times. The ultimate outcome is a curve with infinitely intricate underlying structure which is not differentiable at any point. The generator will replace all straight segments of geometry. The initiator is square as displayed in the Figure (4.9) along with the first three construction iterations [78].

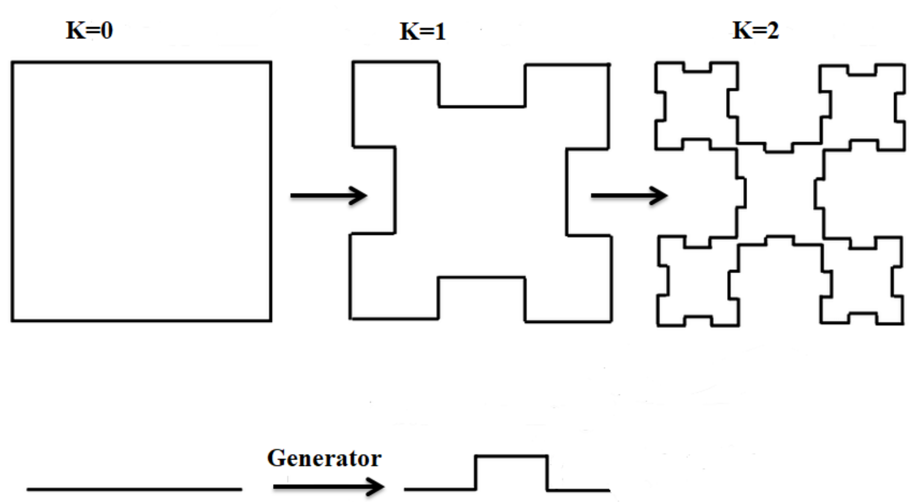

Figure 4.9: The generation of Minkowski island fractal [35], [78].

4.4.5 Hilbert Curve

The first four iterations with initiator of Hilbert curves are displayed in Figure (4.10). It could be noticed that the geometry at a step could be acquired by putting together 4 copies of the preceding iteration, linked to additional line segments. A lot of Hilbert pre-fractal based structures were suggested for producing printed and micro-strip dipole and monopole antennas with compact size and multi-band performance for various implementations [79]

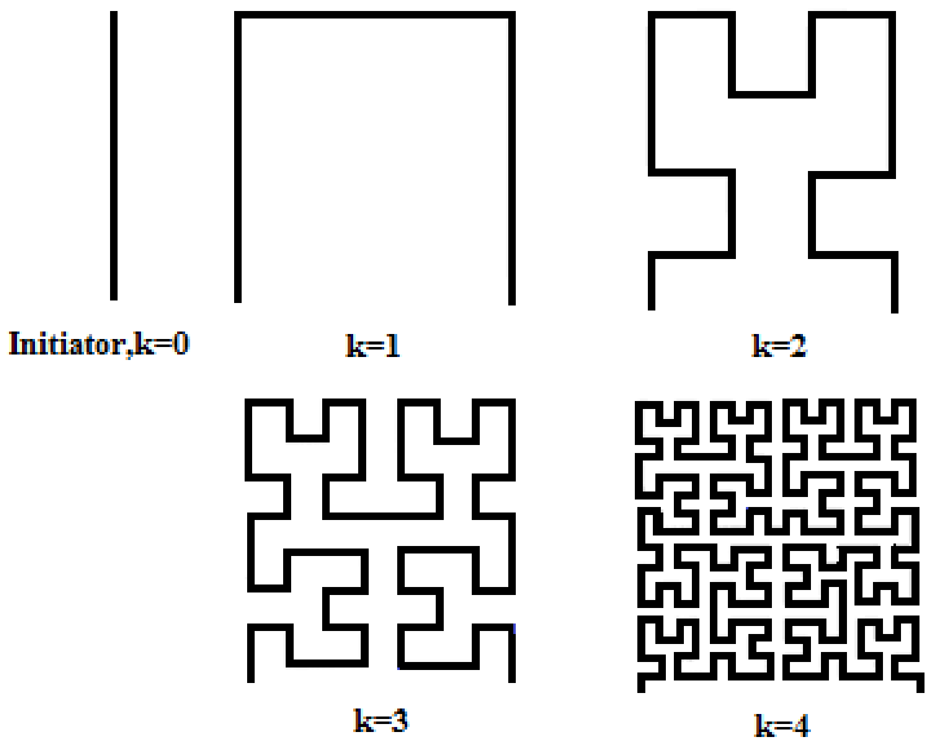

Figure 4.10: The generation of Hilbert curve [31], [79].

4.4.6 Peano Curve

The initiator regarding Peano curve is again specified via a straight line and the correspondent generator include 9 lines one-third of initiator. The first generator’s line runs horizontally, the second turns up 90 degrees, after that, a horizontal segment follows prior to when the curve turns down by 90°. The fifth line move back to the end of the first line with no touching between them. The following part of the curve heads down by 90 degrees, followed by a horizontal part prior to the time where it goes up again. Finally a line located in horizontal position once more forms the last part, as shown in Figure (4.11) .This type is used in antenna design as a modified structure in [80].

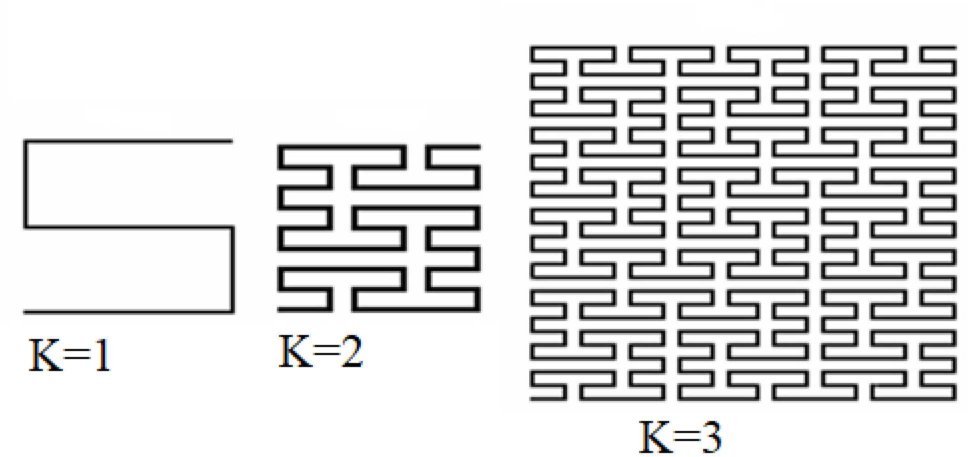

Figure 4.11: The first three iterations levels to construct the Peano pre-fractal curve [80].

Micro-strip fix receiving wires examination strategies have gone through a long handle of improvement. Micro-strip fix received wire examination could be an exceptionally prevalent strategy in conjunction with transmission line show, depth show, and full wave demonstrate [77], and incorporates basically fundamentally equations/Moment Strategy. In common, the transmission line model can be considered as the best of all and it gives great physical knowledge but it isn't as exact. On the other hand, depth demonstrate is more exact and gives great physical knowledge but is complex in nature. Too, full wave demonstrate can be considered the foremost exact, flexible and with the capability of taking care of single components, limited and unbounded clusters, stacked components, subjective formed components and coupling, but, this show is considered on a very basic level complex.

5. DESIGN METHODOLOGY AND THEORY

5.1 INTRODUCTION

With the recent growth in microwave systems, more advanced materials in electromagnetic field applications are demanded. The emergence and development of the concept of "metamaterials" throughout the year led to a revolution and received great interest from researchers [81]. Metamaterial (MTM) is artificial composite materials that have been engineered in precise shape to give it smart properties have the ability to manipulate electromagnetic waves by enhancing, bending, absorbing or blocking waves, to achieve benefits unavailable in natural materials [82]. MTM structures have introduced in various antenna applications including defective ground planes, frequency selective surfaces, artificial magnetic conductors, and perfect lenses [83], to obtain a low profile, higher isolation, SAR Reduction, gain enhancement, improved radiation performance, and unidirectional antenna [84]. Moreover, MTMs possess unique features such as high absorbency capacity, distinctive stopbands, surface wave reduction, and negative effective constitutive parameters [85]. The antennas can be used for medical implants and in-vivo communication [86]. When designing compact portable antennas for employment as part of the wearer's clothes, a lot of needs to be a consideration. Wearable sensors should be safe, flexible, and unobtrusive and operate nearby to the human body with the least possible deterioration [87].

There are some tricky facing the production of wearable antennas, influence of a host body, the work on various body sites, and due to the structural deformation that causes loss of efficiency and reliability, these challenges, should be addressed during the design stage [88]. Thereafter, a critical issue in designing a wearable antenna is the choice of substrate material [89]. It is recommended that the substrate should be a low loss material in order to increase the reliability and gain of the antenna when used near the body. Due to the narrow bandwidth that is determined by the thickness of the substrate, Microstrip antennas are not favorable for applications that demand a high level of rolling, pressure, and bending [90].

In this chapter, we present a new structure reconfigurable wearable antenna based on the metamaterial with radiation pattern end-fire at 2.4 GHz ISM band. The proposed antenna is consists of a traditional monopole coupled with a unit cell of a fractal Minkowski curve to generate three bands frequency spectra to cover different application bands.

5.2 Antenna Geometry

The proposed antenna is constructed from a traditional monopole and a fractal Minkowski-shaped with a Chebyshev transformer. The monopole antenna is fed by 50 Ω port that is located between the monopole conductor and right CPW side, see Figure 1, to keep the directivity toward a certain direction. This is considered to maintain the antenna radiation away from the human body which is a desirable requirement in wearable applications [88]–[91]. The other side of the CPW is constructed as a Chebyshev transformer to improve the impedance matching as well as to enhance the antenna bandwidth. The proposed Chebyshev transformer is an impedance matching circuit that is constructed from 4 stages to maintain different impedances over wide frequency bands.

Now, to ensure the monopole directivity away from human body, we proposed an EBG layer of a 3×4 array. Moreover, the proposed EBG layer is conducted to enhance the antenna gain [92], the quality factor, and the number of resonances in the frequency band of interest because the fractal geometry [85]. Therefore, the proposed EBG is consistent of the Minkowski-shaped fractal unit cell of the 3rd order. The dimensions of the individual unit cell in terms of outer area is 8.5 x 8.5 mm2 with the separation distance between each consecutive is 0.5mm. The proposed EBG layer is placed at a 2.5mm distance from the monopole edge to maintain a frequency band from 2.32GHz up to 2.82GHz.

The antenna substrate is considered as an FR4 layer with 1.6mm thickness. The antenna metal is printed on a single side from the substrate and the other side has been left without metallization as seen in Fig. 5.1. All dimensions are measured in millimeters (mm).

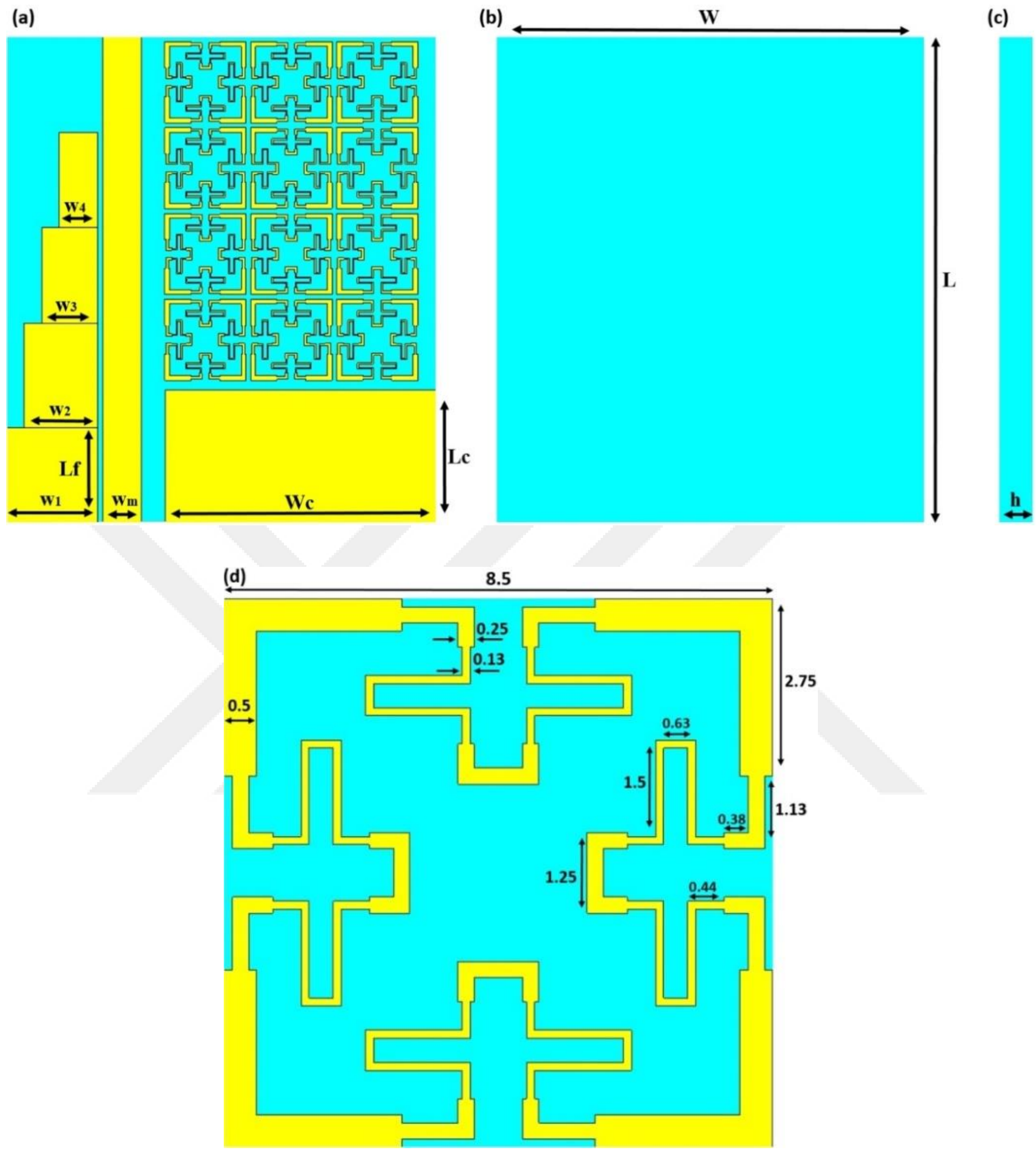

Figure 5.1: The antenna geometrical: (a) front view, (b) back view, and (c) side view, (d) unit cell structure

Table 5.1: Dimensions of the proposed antenna.

Parameter	Value (mm)	Parameter	Value (mm)	Parameter	Value (mm)
L	51	Lc	14	W2	7.7
W	45	Wc	28.42	W3	5.9
h	1.6	Wm	4	W4	4.1

Lf	10	W1	9.5		

5.3 Unit Cell Characterizations

A single unit cell structure of the proposed antenna has examined. The unit cell is made of copper printed on a substrate thickness of 1.6mm. The unit cell is placed inside the waveguide, port on the right side, and another port on the left side to evaluate the S parameters (S_{12} and S_{11}) and obtain the maximum (S_{11}) and the minimum (S_{21}) at the same time. CST MW package was used in the analysis and simulation of a unit cell. It was found that the unit cell operates at a frequency of 2.45 GHz as shown in Figure 5.2.

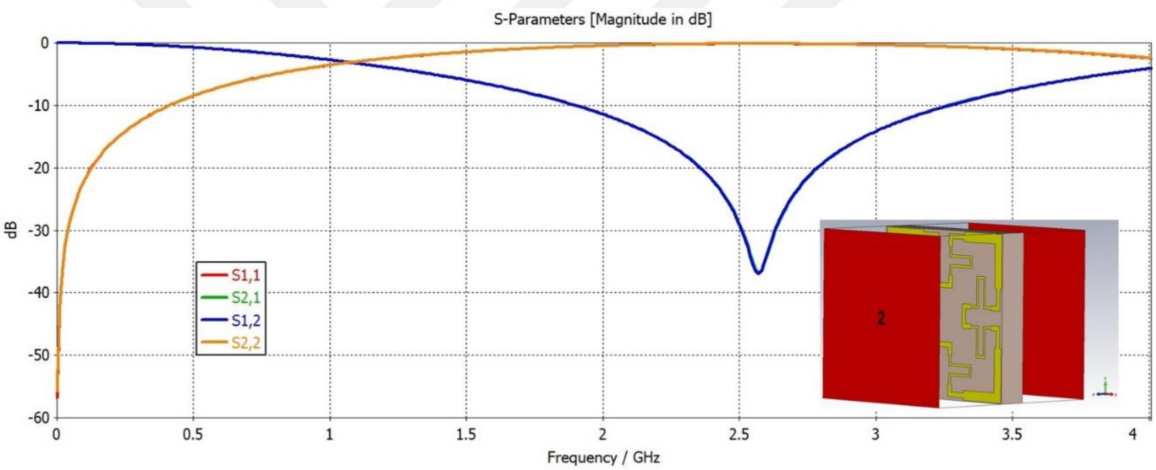

Figure 5.2: S-parameters characterization

5.4 Design Methodology

In this section, a numerical study based on an intensive parametric analysis is conducted by CST MWS [93]. In the proposed parametric study, the performance of the antenna in terms of radiation patterns, boresight gain, and S11 spectra are monitored to arrive the optimal design performance. Therefore, the antenna dimension parameters are swept to maintain two criteria: The first is to obtain three frequency bands around 2.4, 2.7, and 3.4GHz, for ISM band, WLAN, 5G, and IoT applications in portable systems. Then, the second criteria are to keep the antenna radiation away from the human body in specific of the SAR effects reductions on the human tissues. For this, the parametric study is conducted by changing the antenna parameters as following:

5.4.1 Monopole Antenna Design

The authors decided to investigate the stages of the proposed antenna formation. The antenna performance was checked with a conventional monopole and then developed the proposed design by introducing the Transformer into the antenna structure. It was found that the performance of the proposed antenna improved in terms of impedance matching and bandwidth and shift the center frequency towards 2.45 GHz. This is due to the high impedance of the Transformer. In order to improve the parameters of the proposed antenna, the EBG structure has been introduced in the antenna structure. It has been observed that the EBG structure has a significant influence on antenna performance. This improvement is attributed to the reduction of the mutual coupling and surface waves due to the increase in the antenna impedance. As shown in Fig. 5.3 (a).

On the other hand, the proposed design realized three bands at 2.4, 2.7, and 3.4 GHz, which increases the antenna operating range in wireless communication applications.

Now, the investigation study is applied to the proposed monopole length (L) and width (w) to realize their influence on the antenna performance. It is found that the monopole length plays a significant role in antenna performance, therefore, four different monopole lengths are examined, starting from (L = 51mm) to (L = 45 mm) with a step (2 mm) while keeping the other dimensions of the antenna to limit their impact on the performance of the antenna. Fig. 5.3 (b) presents the effects of the length change on the S11 spectra. It is observed from the results of the analysis in Fig. 5.3 (b) by reducing L, the antenna parameters such as bandwidth, resonant frequency, and impedance matching decrease, however, to obtain optimum condition and enhance resonance frequency and impedance matching as well as gain and efficiency in the three bands by tuning L at 51 mm.

(a)

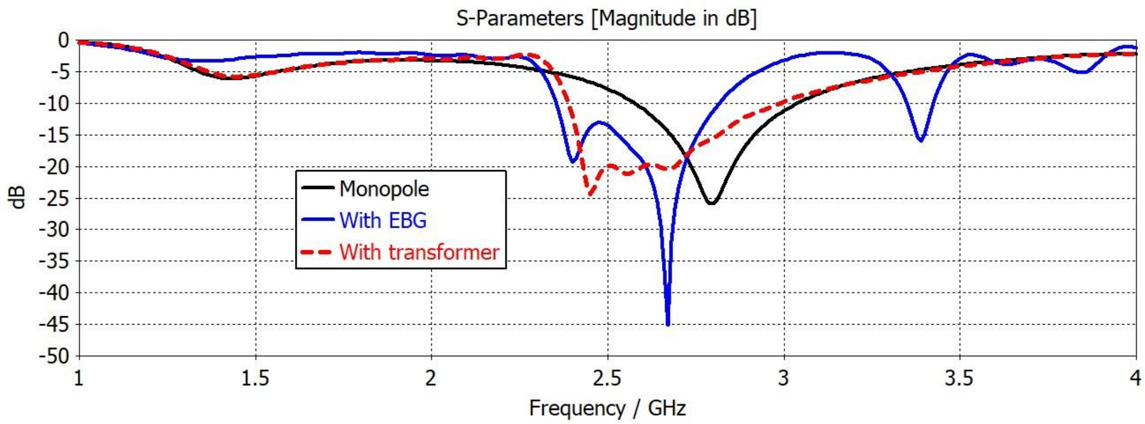

(b)

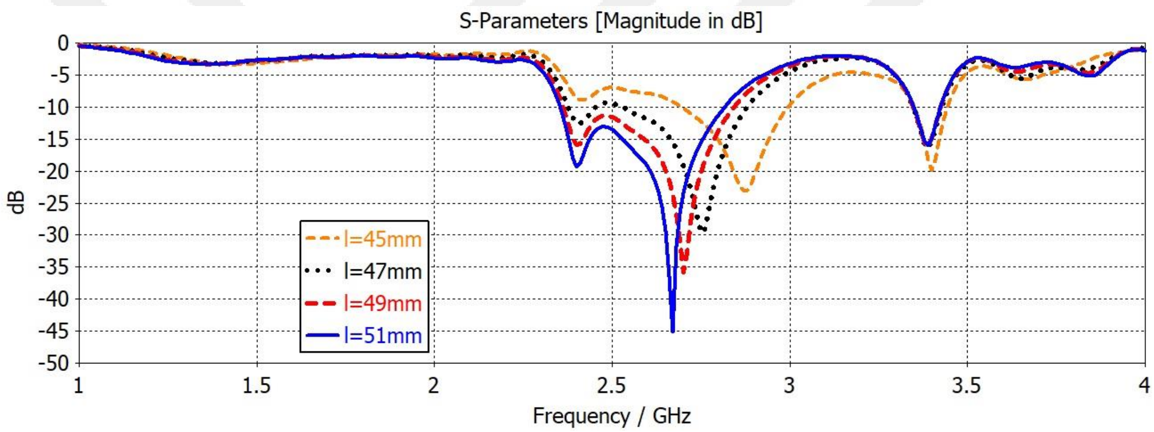

Figure 5.3: (a) Effect of introducing Transformer and EBG structures on antenna design, (b) impact of changing the Monopole length on antenna design.

The Monopole width or length has a significant effect on antenna parameters [94], [95], [96]. Therefore, the authors focus on studying varying of monopole width and effects on the antenna design in terms of, impedance matching, bandwidth, and gain.

Therefore, we variated monopole width W from (5 to 3) mm by a step of (1mm), while keeping the other dimensions of the antenna to cancellate their influence on the antenna behavior. Fig. 5.4 offers the impacts of changing monopole width on the S11 spectra. From the results obtained, a variation in resonant frequency, impedance matching, and bandwidth in the three bands was found due to variation in the monopole impedance and the increase in the mutual coupling between the antenna elements and, consequently, the desired enhance in monopole impedance, as well as the improvement of the antenna performance in the three bands, was achieved by setting W at 4 mm.

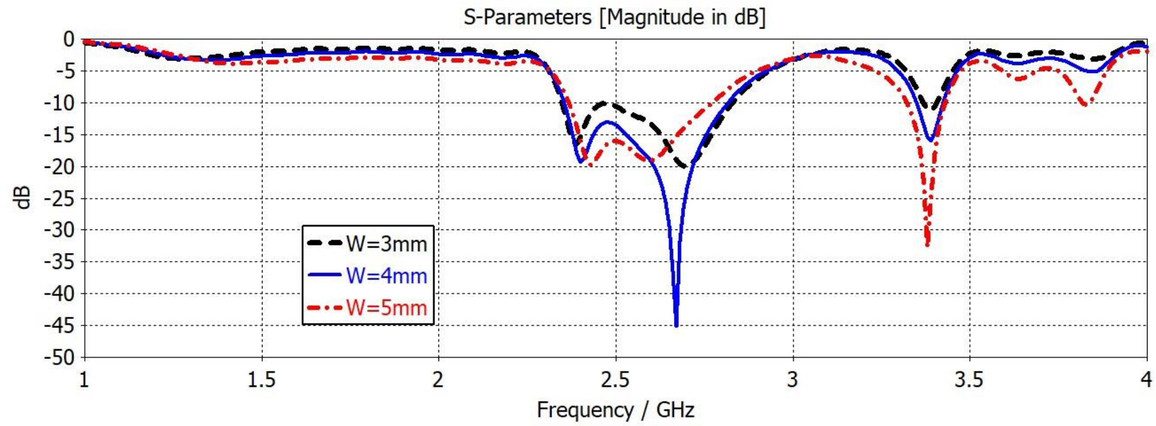

Figure 5.4: Impact of changing the Monopole width on antenna design.

5.4.2 CPW Location Effects

In this part, we examined the impacts of changing the right-wing length on the antenna parameters. Therefore, four lengths have examined starting from (12 to 15) mm in a step of 1 mm, while respect the other antenna dimensions to cancel their influence on the antenna design. Fig. 5.5 displays the effect of the L change on the S11 spectra. The results of the investigation show that changing the CPW length directly affects the performance of the antenna, by increasing or decreasing the length L the resonant frequency is shifted as well as impedance matching was reduced due to the fringing from substrate edge [97], therefore to obtain the optimum condition in terms of impedance matching, bandwidth, and resonant frequency of the three bands when tuning L at 14 mm.

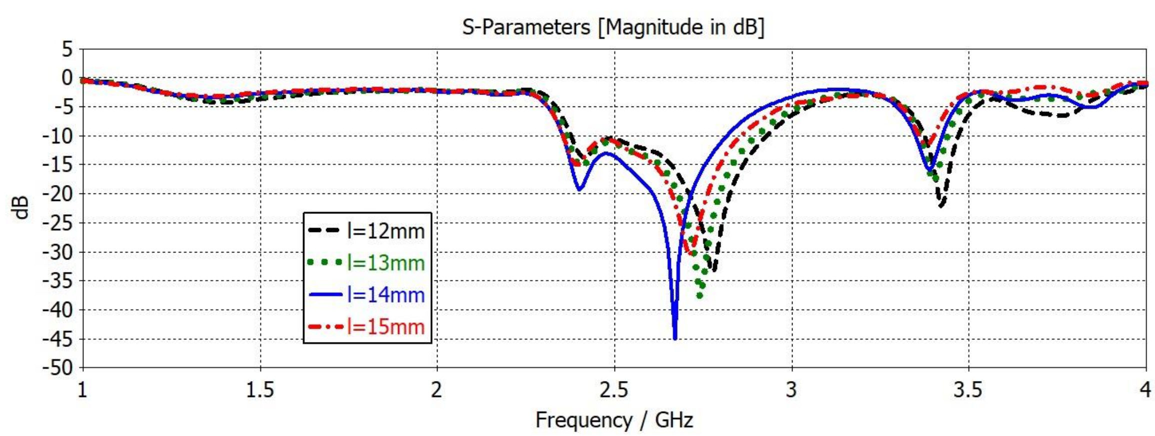

Figure 5.5: Impact of changing CPW length on antenna design.

5.4.3 Chebyshev Transformer Design

In this part, we analyzed the effect of the Chebyshev transformer on antenna performance. It was found that the transformer has a positive effect on the performance of the antenna parameters. Fig. 5.6 (a) offers the impacts of the Chebyshev transformer on the antenna design. It is worth noting that introducing the Chebyshev transformer has a significant effect on the antenna parameters, therefore, the bandwidth and impedance matching significantly improved, furthermore, the antenna covered the entire ISM band due to the appearance of a resonant frequency at 2.4GHz. It is attributed that increased the antenna impedance and reduce mutual coupling [98]. Also, the authors examined the transformer configuration stages and their effects on the antenna behavior such as S11.

The antenna performance was inspected with regard to adding four cases, starting in ascending order from the first to the fourth cases, while keeping the other dimensions of the antenna to limit their impact on the antenna performance. Fig. 5.6 (b) offers the Influence of transformer inserting phases on the S11 spectra.

It was found that the optimum condition in terms of matching the impedance, bandwidth, and resonant frequency by adding the fourth case, which improves the antenna impedance then enhances the antenna performance, as in Fig. 5.6 (b).

(a)

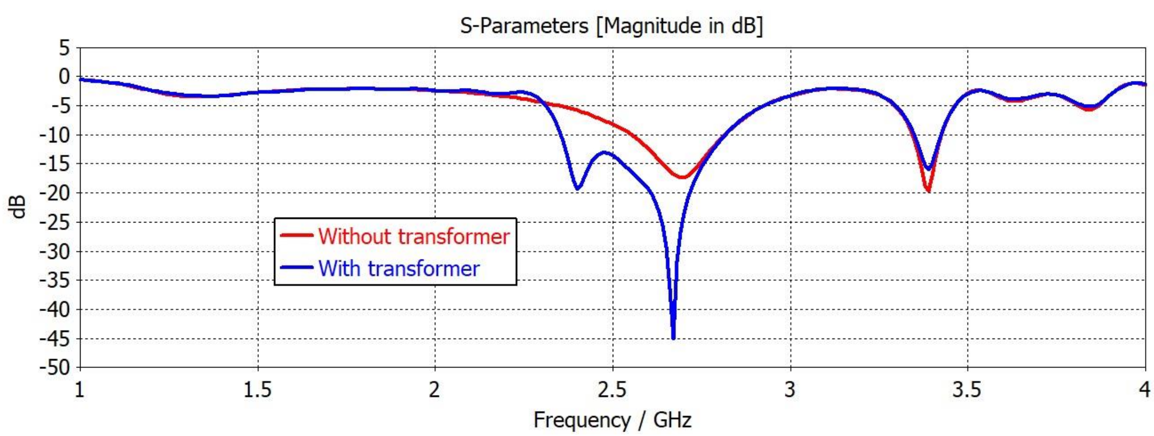

(b)

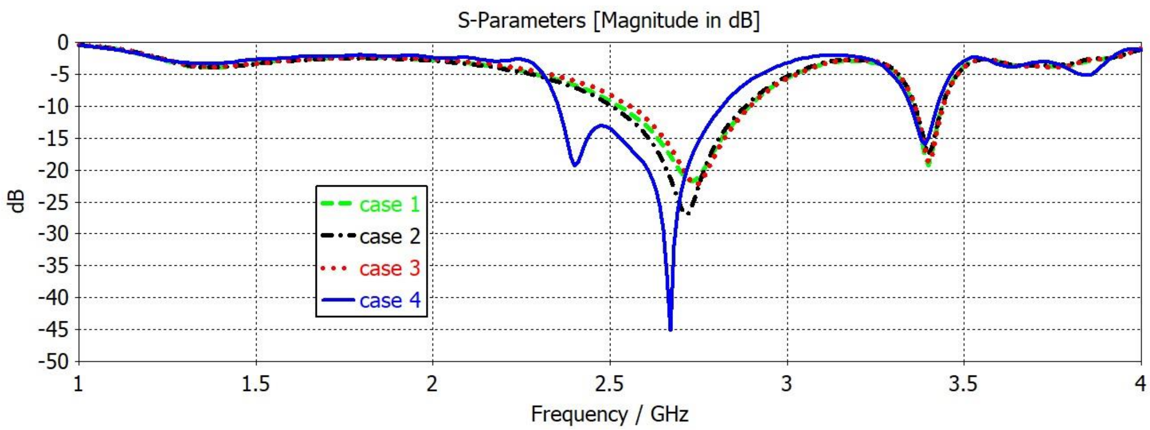

Figure 5.6: Transformer effect: (a) the impact of the transformer on the proposed antenna and (b) impact of transformer configuration stages on the antenna design.

5.4.4 Antenna Performance Based EBG Layer

In this section, we decided to conduct a parametric study on antenna design in order to recognize the antenna performance without unit cell introduction. The results of a study concluded that the proposed antenna achieved good results with excellent matching in terms of resonant frequency at 2.45 GHz and bandwidth of 25.47% from (2.38_3) GHz, | S_{11} | <-10 dB, also, the maximum gain of 2.74 dBi and the antenna efficiency of 80%, see Figure 5.7 the proposed antenna without EBG.

Also, the direction of the antenna radiation emitting from the patch is keeping away from the human body in specific of the SAR effects reductions on the human tissues. Table 5.2, the effect of inserting EBG on the performance of the proposed antenna.

On the other hand, after the introduction of EBG structures, it has observed a significant effect on antenna performance [99], where three frequency bands appeared at 2.4, 2.7, and 3.4 GHz, which increased the antenna operating ranges in wireless communication systems.

Also, a significant improvement in the gain, efficiency, and directivity of the radiation pattern of the proposed antenna.

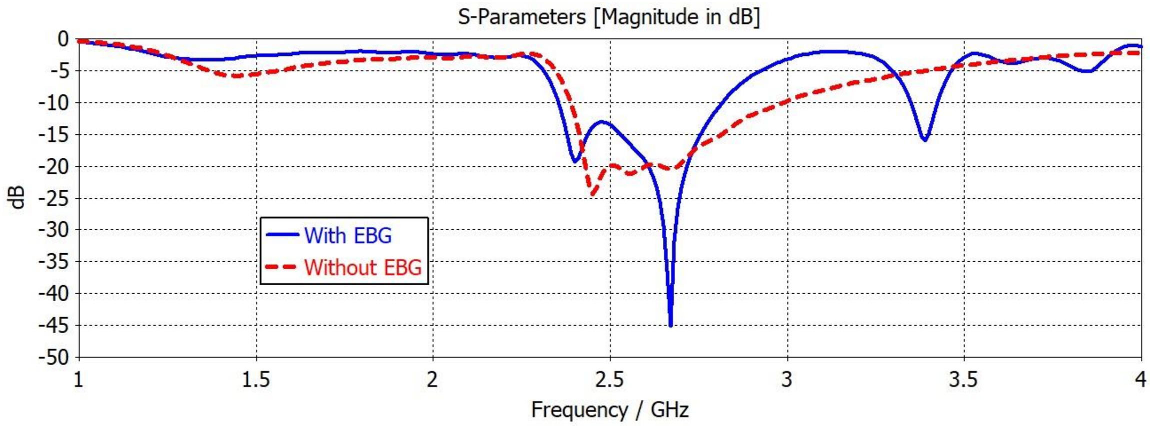

Figure 5.7: Antenna performance Without EBG structure.

MTM structure plays an important role in improving the antenna parameters [92], therefore, in order to recognize the benefits of introducing a cell unit to the performance of the antenna, the authors in this work conducted a parametric study focusing on the use of MTM structure in the design of the proposed antenna, the unit cell contains an (EBG), number of these gaps and their influence on antenna behavior has investigated in this section.

Moreover, the authors examined the effects of rows, and columns of the unit cell printed on the same substrate surface and located 2.5mm from the monopole edge. Due to the restriction of the substrate boundaries, the number of unit cell structures used in the proposed antenna design is four rows and three columns. Results: The use of the unit cell structure leads to enhance the performance antenna in terms of gain, efficiency, and operating range, which is attributed to the decrease in mutual coupling due to the high impedance in the unit cell thus the surface waves are reduced. Furthermore, it is found that the impedance matching has been improved by adding four arrays, see Figure 5.8. Because reflecting energy from the EBG structure toward the monopole antenna.

From the above discussion, the authors conclude that the antenna realized the required performance by using a 3x4 array of unit cell structures. Table 5.2 shows the effect of EBG on the proposed design.

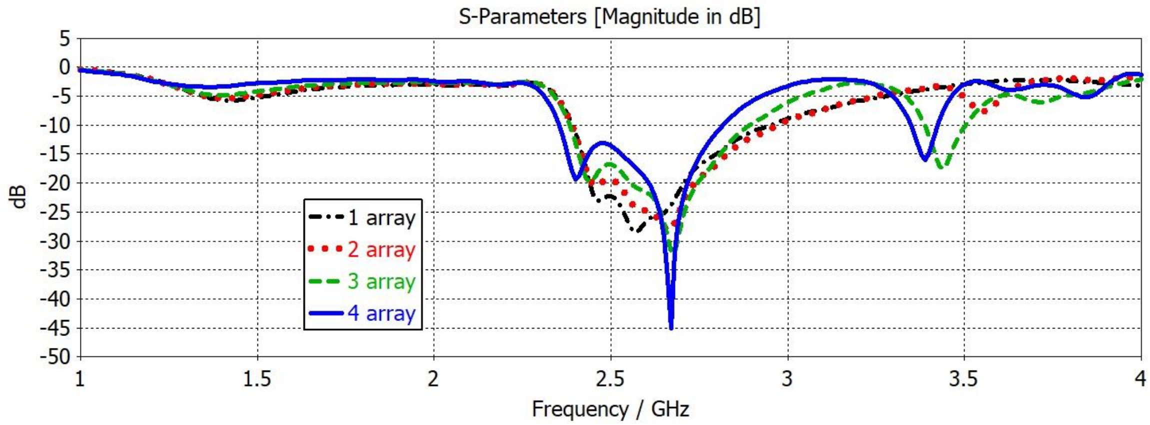

Figure 5.8: Impact the EBG array on S11 spectra.

Table 5.2: The effect of inserting EBG on the performance of the proposed antenna.

Parameters	Without EBG *f 1*	Without EBG *f 2*	With EBG *f 1*	With EBG *f 2*	With EBG *f 3*
Frequency (GHz)	2.45	2.7	2.4	2.7	3.4
Bandwidth (MHz)	620		500		80
Gain (dBi)	2.74	2.61	4.93	5	1.5
Antenna efficiency %	80.6	95.5	93	93.8	60.3

After investigating the effect of EBG on antenna performance, we decided to examine the influence of the distance between monopole and unit cell arrays in terms of resonant frequency, bandwidth, and matching impedance on the behavior of the proposed antenna.

Therefore, the distance (m) has changed from 2.5mm to 4.5mm with a step of 1 mm while keeping the other antenna dimensions to cancel their influence on the antenna design. From Fig. 5.9, it is found that the distance between the unit cell and the monopole has a significate effect on the S_{11} spectra, due to the effects of mutual coupling and the surface waves that decrease when the distance between the unit cell structure and the monopole edge small [90]. we point that the ideal state in terms of resonance frequency, impedance matching, and bandwidth when set distance (m) to 2.5mm.

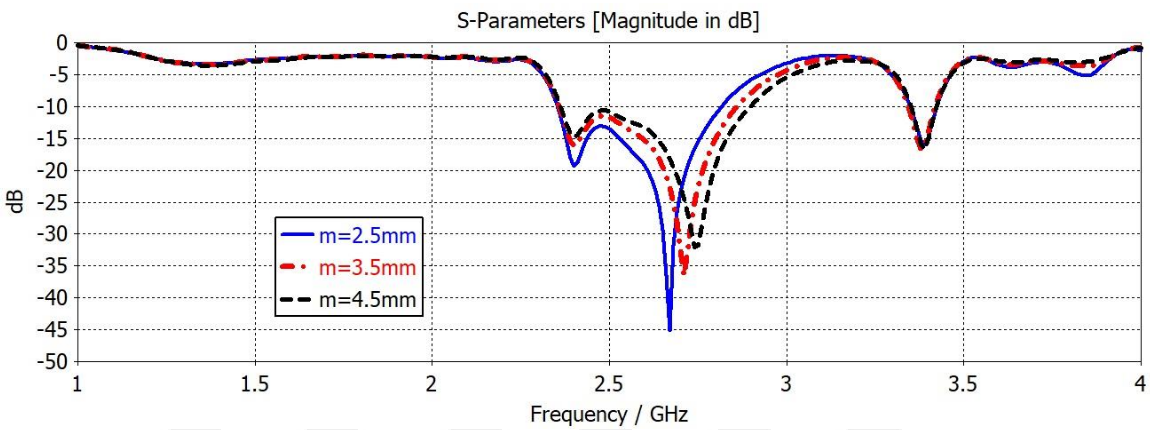

Figure 5.9: Distance impact between unit cell structure and Monopole on S_{11} spectra.

5.4.5 Effect of a PIN Diode on Antenna Performance

After analyzed the antenna performance to obtain the optimum condition of the design, now in this section, the authors have attempted to controllable the behavior of the proposed antenna by inserting a PIN diode into the lower edge between the monopole and the transformer. Using a PIN diode, the proposed antenna achieved the potential of reconfiguring the radiation pattern by blocking the ISM band frequencies (PIN diode ON) while maintaining | S_{11} | <-10dB and resonant frequency at two bands 2.7, 3.4 GHz, with an impedance bandwidth of 330 MHz (2.83 _ 2.5GHz), 80MHz (3.346_3.4264GHz) respectively. Figure 5.10 presents the influence of PIN diode on S_{11} spectra. Lumped elements values were set and simulated using the CST MWS package, as shown in Table 5.3.

Also, in the case of PIN diode switch (SW OFF), it was found that the performance of the proposed antenna has improved in terms of bandwidth, gain, and efficiency at two modes 2.4 and 2.7 GHz with maintaining the resonant frequency at 3.4GHz. This is due to the good insulation between the antenna elements and the PIN diode position, which plays an important role in reconfigurable the antennas [100], [101].

Therefore, the antenna has achieved an impedance bandwidth of 500 MHz (2.32 - 2.82GHz) at 2.4GHz and radiation efficiency at the two modes (2.4, 2.7 GHz) of 96.2% and 94.2% respectively.

This improvement is attributed to the increase in the impedance of the proposed antenna due to the decrease in the mutual coupling between the antenna and the transformer [98]. Table 5.4 offers the effect of introducing the PIN diode on antenna performance.

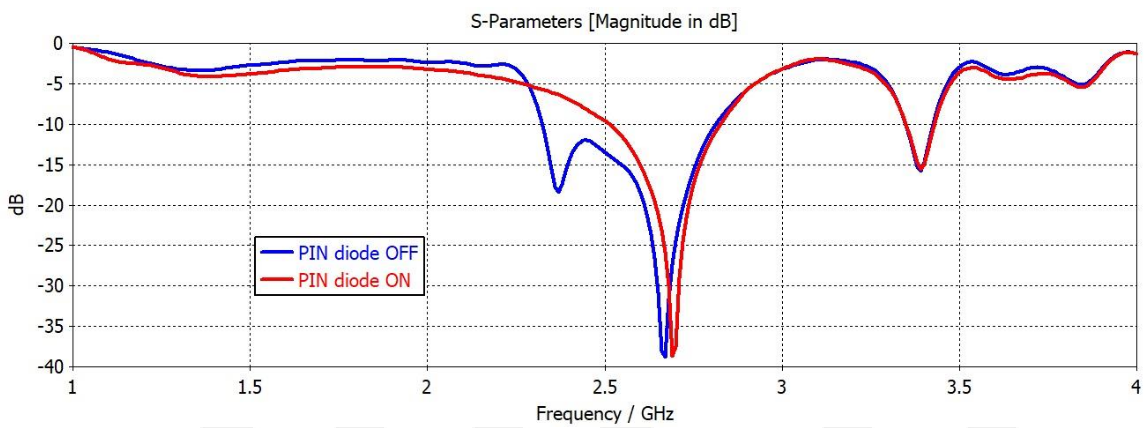

Figure 5.10: Effect of PIN diode introduce on S_{11} spectra.

The proposed antenna has a wide range and high efficiency, which makes it suitable for work in wireless communication systems applications, such as WBAN, Bluetooth, and WLAN.

Table 5.3: Lumped elements values.

PIN diode status	Resistor (R)	Inductor (L)	Capacitor (C)
ON	3Ω	2.6×10^{-13}H	0F
OFF	20KΩ	0H	40pF

Table 5.4: Simulated the effect of the PIN diode on the antenna parameters.

Antenna condition	Frequency (GHz)	$\|S_{11}\|$ (dB)	Bandwidth (MHz)	Gain (dBi)	Efficiency %
Without PIN diode	2.4	-19.38	470	4.73	87.63
	2.7	-45.11		4.85	92.21
	3.4	-16	80	1.5	60
PIN diode (SW ON)	2.7	-38.5	330	4.6	93.22
	3.4	-15.5	80	1.5	61.1
PIN diode (SW OFF)	2.4	-18.3	500	4.93	92.87
	2.69	-38.8		5	93.87
	3.4	-15.5	80	1.48	60.3

6. RESULTS AND DISCUSSION

In this section, the proposed antenna simulation results are presented in terms of radiation pattern, reflection coefficient, impedance bandwidth, efficiency, and gain. CST MWS package was used to simulate the antenna. Figure 5.10 shows the effect of introducing the PIN diode on the antenna designed in terms of impedance bandwidth and reflection coefficients under the PIN diode ON and OFF conditions.

In the case of the (SW ON), the ISM band is isolated and the antenna covers two bands, the first, in Wi-Fi bands (2.5 - 2.83 GHz) with a center frequency of 2.7 GHz and an impedance bandwidth of 12.2%, and the second in WLAN bands with a resonant frequency at 3.4GHz. In the case (SW OFF), the proposed antenna operates in three bands 2.4, 2.7, and 3.4GHz, covering ranges (2.32 - 2.82 GHz), (3.346_3.4264GHz) respectively.

In both cases (switching ON and OFF) the proposed antenna achieved acceptable performance compared to previous related literature. Figure 5.11 shows the radiation patterns of the designed antenna. The radiation patterns are evaluated based on E-plane (Phi = 0), and H-plane (Phi = 90) at (SW ON and OFF). The radiation patterns of the proposed antenna are found at (Phi = 0) and (Phi = 90) in the desired direction away from the human body, therefore electromagnetic waves travel in specific directions, thus reducing the specific absorption rate (SAR) and their effects on human tissues.

In the case of (SW ON), the proposed antenna realized a gain of 4.6 and 1.5 dBi at 2.7, 3.4 GHz with an efficiency of 93.2%, 61.1% respectively, while in the case of (SW OFF) the gain of the antenna reached 4.93, 5, and 1.48 dBi with an efficiency of 92.8%, 93.8%, 60.3% at three bands 2.4, 2.7, and 3.4 GHz, as in Figure 5.12. The improvement of the antenna gain is attributed to the role of EBG structure in reducing surface waves and the mutual coupling between the antenna elements.

The surface current distributions of the designed antenna are investigated. Therefore, it is observed that in the case of PIN diode switching ON at 2.7 and 3.4GHz, the surface current is concentrated at the lower edge of the monopole and moves towards the CPW structure, however, by switching OFF at 2.4, 2.7, and 3.4GHz, the surface current moves towards the transformer as seen in Figure 5.13.

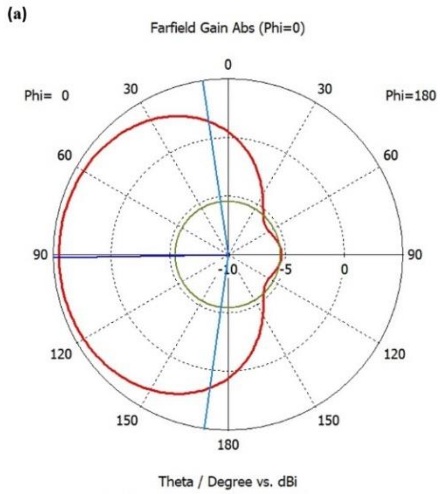

E-plane (f=2.7GHz), SW=ON

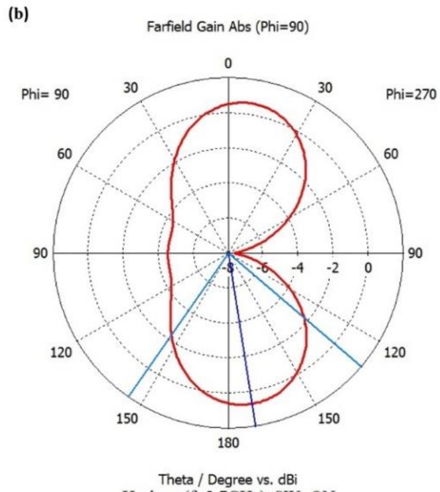

H-plane (f=2.7GHz), SW=ON

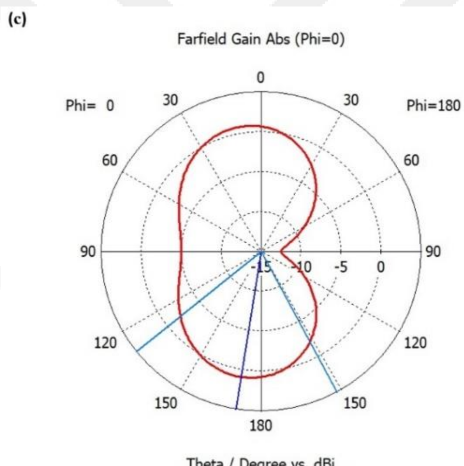

E-plane (f=3.4), SW=ON

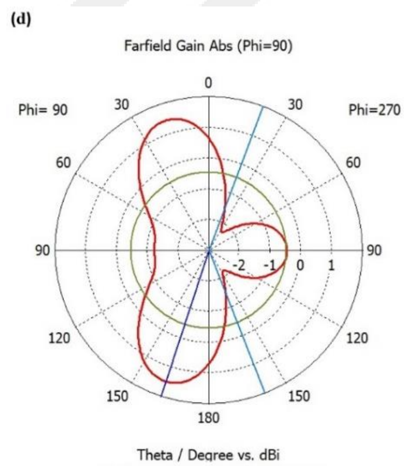

H-plane (f=3.4GHz),SW=ON

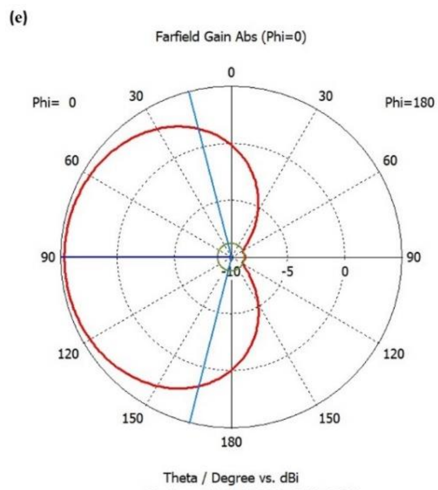

E-plane (f=2.4GHz), SW=OFF

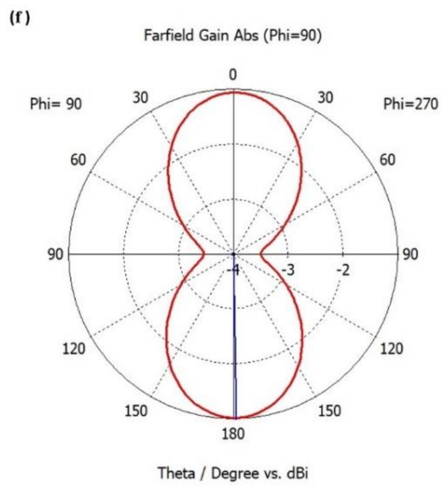

H-plane (f=2.4GHz), SW=OFF

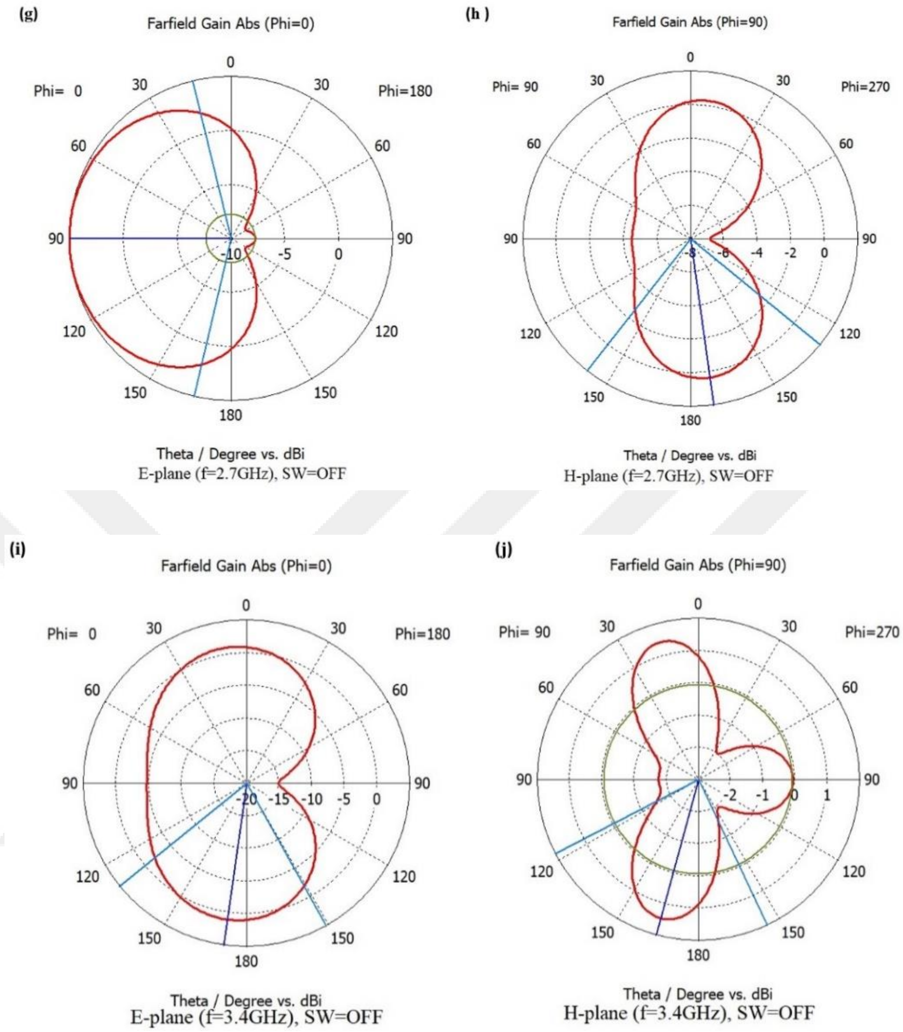

Figure 6.1: Simulated E-plane and H-plane radiation patterns of the proposed antenna: (a), (b), (c), (d) when PIN diode ON, while (e), (f), (g), (h), (i), (j) when PIN diode OFF.

(a)

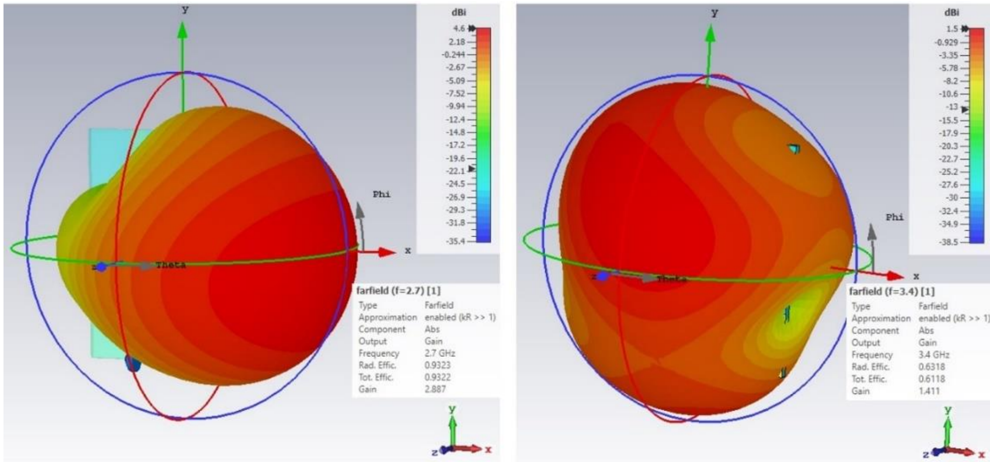

(b)

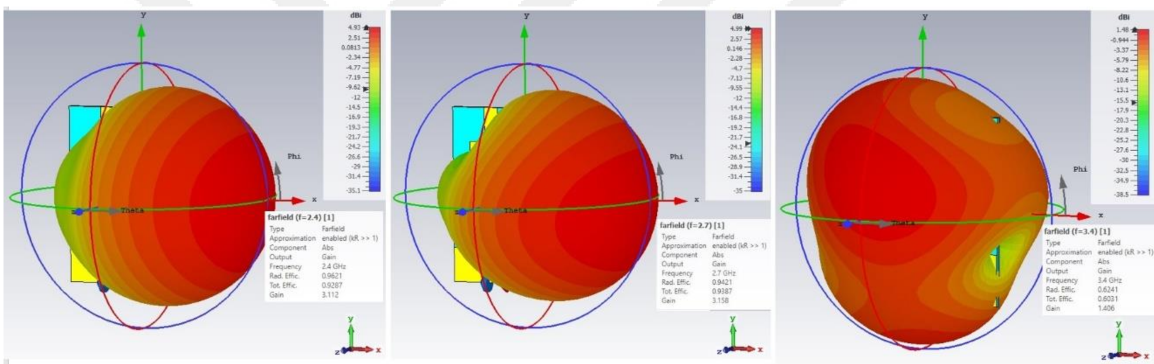

Figure 6.2: Simulated 3D radiation patterns of the proposed antenna: (a) PIN diode SW=ON (2.7GHz, 3.4GHz), while (b) PIN diode SW=OFF (2.4GHz, 2.7GHz, and 3.4GHz)

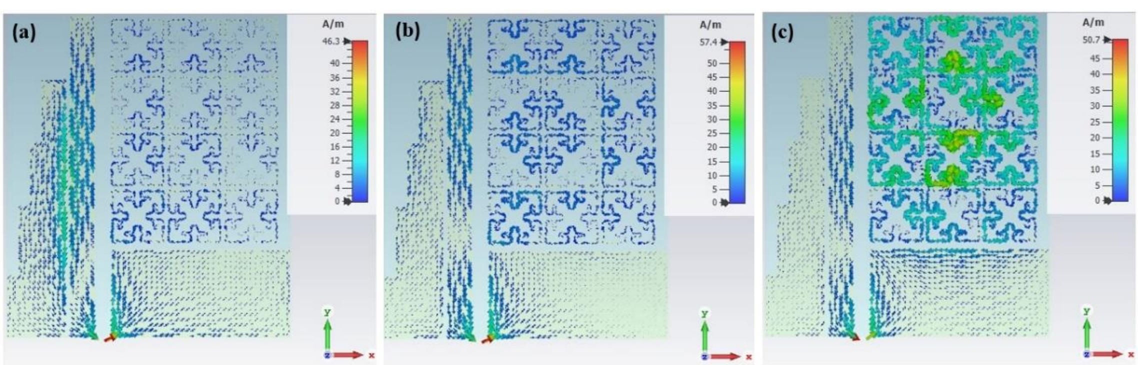

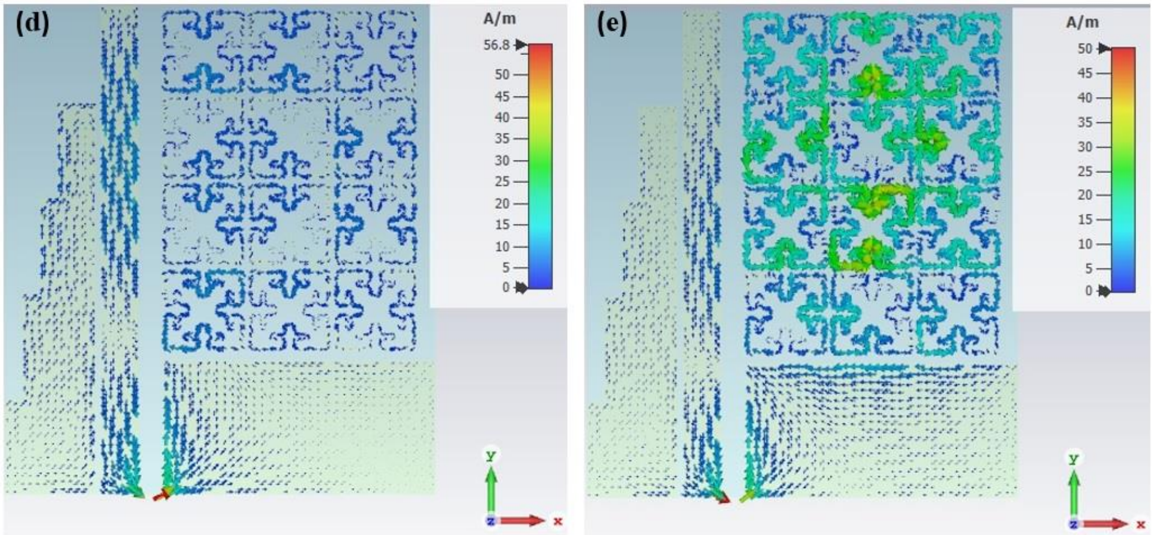

Figure 6.3: Current distribution of the proposed antenna: (a), (b), (c) PIN diode SW=OFF (2.4, 2.7, and 3.4GHz) respectively, while (d) and (e) PIN diode SW=ON (2.7 and 3.4GHz).

7. CONCLUSIONS AND FUTURE WORKS

7.1 CONCLUSIONS

In this thesis, a novel wearable reconfigurable antenna based on the metamaterial has been introduced for (WBAN) and WLAN applications. The antenna structure has been developed by introducing the Chebyshev Transformer in order to increase bandwidth and improve impedance matching. Antenna performance is improved by inserting the EBG structure array in the design of the proposed antenna. Several parametric studies were performed to obtain the optimum design using the CST Microwave Studio package.

The proposed antenna is printed on an inexpensive and available FR4 dielectric substrate in 51x 45 x1.6 mm^3 dimensions and fed to port 50-ohm SAM. After analyzed the antenna performance to obtain the optimum condition of the design, we have attempted to controllable the behavior of the proposed antenna by inserting a PIN diode into the lower edge between the monopole and the transformer. Using a PIN diode, the proposed antenna achieved the potential of reconfiguring the radiation pattern by blocking the ISM band frequencies (PIN diode ON) while maintaining | S11 | <-10dB and resonant frequency at two bands 2.7, 3.4 GHz, with an impedance bandwidth of 330 MHz (2.83 _ 2.5GHz), 80MHz (3.346_3.4264GHz) respectively. Lumped elements values were set and simulated using the CST MWS package.

Also, in the case of PIN diode switch (SW OFF), it was found that the performance of the proposed antenna has improved in terms of bandwidth, gain, and efficiency at two modes 2.4 and 2.7 GHz with maintaining the resonant frequency at 3.4GHz. This is due to the good insulation between the antenna elements and the PIN diode position, which plays an important role in reconfigurable the antennas.

The antenna achieved reconfiguration by introduced a PIN diode into the lower edge between the Transformer and the Monopole. The proposed antenna achieved good results and the end-fire radiation pattern in both cases (SW= ON, OFF). The antenna performance has compared with previous work. It was found that the performance of the proposed antenna is good and suitable for wearable applications.

7.2 FUTURE WORKS

1. The proposed design is conducted based on an FR-4 substrate. However; as a future study, the author is attempt the study on a flexible substrate to provide high efficiency, reliability, durability, and size reduction.

2. The author used the third-order fractal Minkowski structure, therefore, the subject for this research in the future to apply another Matrix structure to reach further bands including 5.8GHz for RFID and Wi-Fi applications.

3. The antenna is fabricated using a copper layer etched from an FR4 substrate; however, in future work, utilize printing technology-based nanoscale conductive ink to fabricate the proposed antenna.

4. The author used the Chebyshev transformer to provide excellent matching impedance, therefore, in the future, another transformer is subjected to be used for this design.

5. The antenna design will be fabricated on a flexible substrate to be suit for wearable applications and bending scenarios.

6. The use of ground plane defects would be another approach for enhancing the antenna performance using EBG and MTM structures.

7. The proposed work would be extended to include a Fabricate and Measure the designs.

8. REFERENCES

[1] S.J. Chen, and D.C. Ranasinghe, “A modular textile antenna design using snap-on buttons for wearable applications,” IEEE Transactions on Antennas and Propagation, vol. 64, no. 3, March 2016.

[2] C. Mohan and S. E. Florence, ``Miniaturised triangular microstrip antenna with metamaterial for wireless sensor node applications," IETE J. Res., pp. 1_6, Jul. 2019.

[3] Y. J. Li, Z. Y. Lu, and L. S. Yang, ``CPW-fed slot antenna for medical wearable applications," IEEE Access, vol. 7, pp. 42107_42112, 2019.

[4] Hu, J., “Overview of flexible electronics from ITRI’s viewpoint,” *2010 28th VLSI Test Symposium*.

[5] S. Velan, E. F. Sundarsingh, M. Kanagasabai, A. K. Sarma, C. Raviteja, R. Sivasamy, and J. K. Pakkathillam, ``Dual-band EBG integrated monopole antenna deploying fractal geometry for wearable applications," IEEE Antennas Wireless Propag. Lett., vol. 14, pp. 249_252, 2015.

[6] A. Y. I. Ashyap, Z. Zainal Abidin, S. H. Dahlan, H. A. Majid, M. R. Kamarudin, A. Alomainy, R. A. Abd-Alhameed, J. S. Kosha, and J. M. Noras, ``Highly efficient wearable CPW antenna enabled by EBG- FSS structure for medical body area network applications," IEEE Access, vol. 6, pp. 77529_77541, 2018.

[7] S. A. A. Shah and H. Yoo, ``Scalp-implantable antenna systems for intracranial pressure monitoring," IEEE Trans. Antennas Propag., vol. 66, no. 4, pp. 2170_2173, Apr. 2018.

[8] L. W. Liu, A. Kandwal, Q. Cheng, H. Shi, I. Tobore, and Z. Nie, ``Non-Invasive blood glucose monitoring using a curved Goubau line," Electronics, vol. 8, no. 6, p. 662, Jun. 2019.

[9] A. Sharma, E. Kampianakis, and M. S. Reynolds, ``A dual-band HF and UHF antenna system for implanted neural recording and stimulation devices," IEEE Antennas Wireless Propag. Lett., vol. 16, pp. 493_496, 2017.

[10] M. Suzan Miah, A. N. Khan, C. Icheln, K. Haneda, and K.-I. Takizawa, ``Antenna system

design for improved wireless capsule endoscope links at 433 MHz," IEEE Trans. Antennas Propag., vol. 67, no. 4, pp. 2687_2699, Apr. 2019.

[11] A. Basir and H. Yoo, ``A stable impedance-matched ultrawideband antenna system mitigating detuning effects for multiple biotelemetric applications," IEEE Trans. Antennas Propag., vol. 67, no. 5, pp. 3416_3421, May 2019.

[12] A. Pourghorban Saghati, J. Singh Batra, J. Kameoka, and K. Entesari, ``Miniature and reconfigurable CPW folded slot antennas employing liquid-metal capacitive loading," IEEE Trans. Antennas Propag., vol. 63, no. 9, pp. 3798_3807, Sep. 2015.

[13] J. Kula, D. Psychoudakis, W.-J. Liao, C.-C. Chen, J. Volakis, and J. Halloran, ``Patch-antenna miniaturization using recently available ceramic substrates," IEEE Antennas Propag. Mag., vol. 48, no. 6, pp. 13_20, Dec. 2006.

[14] S. Agneessens, S. Lemey, T. Vervust, and H. Rogier, ``Wearable, small, and robust: The circular quarter-mode textile antenna," IEEE Antennas Wireless Propag. Lett., vol. 14, pp. 1482_1485, 2015.

[15] H. Wong, K. K. So, K. B. Ng, K. M. Luk, C. H. Chan, and Q. Xue, ``Virtually shorted patch antenna for circular polarization," IEEE antennas Wireless Propag. Lett., vol. 9, pp. 1213_1216, 2010.

[16] C. Liu, Y.-X. Guo, and S. Xiao, ``Capacitively loaded circularly polarized implantable patch antenna for ISM band biomedical applications," EEE Trans. Antennas Propag., vol. 62, no. 5, pp. 2407_2417, May 2014.

[17] Elwi TA (2017), "A miniaturized folded antenna array for MIMO applications". Wireless Pers Commun 98: 1871-1883.

[18] Hazarika, B., B. Basu, and A. Nandi, “Design of antennas using artificial magnetic conductor layer to improve gain, flexibility, and specific absorption rate,” Microwave and Optical Technology Letters, Vol. 62, No. 12, 3928–3935, 2020.

[19] A. Hashemi, S. Nourbakhsh, P. Tehrani and A. Karimi,”Remote telemonitoring of cardiovascular patients: Benefits, barriers, new suggestions”, Artery Research, vol. 22, pp. 57-63, 2018.

[20] N. Mohammadzadeh and R. Safdari, Patient Monitoring in Mobile Health: Opportunities and Challenges, Med. Arch., vol. 68, no. 1, pp. 5760, 2014.

[21] B. B. Zaidan, A. A. Zaidan, M. Hashim, H. Muzammil, O. H. Salman, and N. Kalid, Based 35Real Time Remote Health Monitoring Systems: A Review on Patients Prioritization and Related Big Data Using Body Sensors information and Communication Technology, J.Med. Syst., vol. 42, no. 2, pp. 130, 2017.

[22] Sopa, P. and P. Rakluea, “The hexagonal shaped UWB wearable textile antenna with band-notched characteristics,” 2020 8th International Electrical Engineering Congress (iEECON), IEEE, 2020.

[23] Garg, R., et al., Microstrip Antenna Design Handbook, Artech House, 2001.

[24] L. Belrhiti, F. Riouch, A. Tribak, J. Terhzaz, and A. M. Sanchez, Flexible Antennas Design and Test for Human Body Applications Scenarios, J. Microwaves, Optoelectron. Electromagn. Appl., vol. 16, no. 2, pp. 494513, 2017.

[25] J. K. Ali, Seevan F. Abdulkareem, Ali I. Hammoodi, and Hussain Al-Rizzo, "Cantor fractal-based printed slot antenna for dual-band wireless applications", March 2016, International Journal of Microwave and Wireless Technologies, DOI: 10.1017/S1759078714001469.

[26] J. Dalfiah and D. Karuppasamy, "Design of split-ring resonator embedded metamaterial monopole antenna for short-range communication", (ICEI) IEEE, 11-12 May 2017, DOI: 10.1109/ICOEI.2017.8300773.

[27] Omar. M. Khan, R. Shubair, and Q. Ul. Islam, "Second-Order Flamenco Fractal Antenna for Industrial Scientific and Medical Applications", (ICECTA) IEEE, 21-23 Nov. 2017, DOI: 10.1109/ICECTA.2017.8252031.

[28] S. Roy and U. Chakraborty, "Metamaterial Based Dual Wideband Wearable Antenna for Wireless Applications", June 2019, Wireless Personal Communications, DOI: 10.1007/s11277-019-06206-3.

[29] Hayder. S. Ahmed, T. Elwi, "On the design of a reject band filter for antennas mutual coupling reduction", International Journal of RF and Microwave Computer-Aided Engineering, 24 April 2019, doi.org/10.1002/mmce.21797.

[30] A. Arif, M. Zubair, M. Ali, M. U. Khan and Qasim Mehmood, "A Compact, Low-Profile Fractal

Antenna for Wearable On-Body WBAN Applications", IEEE Antennas and Wireless Propagation Letters (Volume: 18, Issue: 5, May 2019), DOI: 10.1109/LAWP.2019.2906829.

[31] Zainab Al-Dulaimi, T. Elwi, D. C. Atilla, " Design of a Meander Line Monopole Antenna Array Based Hilbert-Shaped Reject Band Structure for MIMO Applications", IETE Journal of Research, 23 Mar 2020, doi.org/10.1080/03772063.2020.1743207.

[32] Arka Bhattacharyya, Amartya Banerjee, Sayan Chatterjee, Bhaskar Gupta, " Dual-Band Minkowski Fractal Patch Antenna With Polarization Diversity", 2020 IEEE Calcutta Conference (CALCON), 02 June. 2020, DOI: 10.1109/CALCON49167.2020.9106540.

[33] Ali Arif, M. R. Akram, K. Riaz, M. Zubair and M. Mehmood, " Koch Fractal Based Wearable Antenna Backed with EBG Plane", IEEE (IBCAST), 14-18 Jan. 2020, DOI: 10.1109/IBCAST47879.2020.9044575.

[34] T. Elwi and Sarah G. Abdulqader, " Further investigation on solant–rectenna-based flexible Hilbert-shaped metamaterials", June 2020, IET Nanodielectrics, DOI: 10.1049/iet-nde.2020.0013.

[35] S. M. Obaid, T. Elwi, and M. Ilyas, " Fractal Minkowski-Shaped Resonator for Noninvasive Biomedical Measurements: Blood Glucose Test", Progress In Electromagnetics Research C, Vol. 107, 143-156, 2021, doi:10.2528/PIERC20072603.

[36] Fractal, Available [online]: http://mathworld.wolfram.com/Fractal.html.

[37] W. L. Stutzman, G.A. Thiele. "Antenna Theory And Design". 3rd ed. John Wiley & Sons, Inc. 2012. pp. 32-36.

[38] R. Bancroft, "Microstrip and Printed Antenna Design", 2nd Ed., SciTech Publishing, Inc., Raleigh, NC, 2009.

[39] S. Bisht, S. Saini, V. Parakash, B. Naitiyal. "Study The Various Feeding Techniques of Microstrip Antenna Using Design and Simulation Using CST Microwave Studio". International Journal Of Emerging Technology And Advanced Engineering. Volume 4, Issue 9. September 2014.

[40] R. Bancraft. "Microstrip And Antenna Design". 2nd ed. SciTech, Inc. 2009. pp. 1-4.

[41] C. A. Balanis. "Antenna Theory: Analysis And Designs". 4th ed. John Wiley & Sons, Inc. 2016.

[42] Muhammad Abdul Samad, Abdul Kadir Hamid, "Miniaturization of Waveguide Antenna Using Square/Circular Arrays Of SRR", IEEE 2016, DOI: 10.1109/ICEDSA.2016.7818474.

[43] A. Kumar, J. Kaur, R. Singh. "Performance Analysis Of Different Feeding Techniques". International Journal Of Emerging Technology And Advanced Engineering. Volume 3, Issue 3. March, 2013.

[44] Hardinata S, Deshours F, Alquié G, Kokabi H, Koskas F. Miniaturization of Microwave Biosensor for Non-invasive Measurements of Materials and Biological Tissues. IPTEK Journal of Proceedings Series. 2018 Jan 29(1):90-3.

[45] E. Ekmekci and G. Turhan-Sayan, “Multi-functional metamaterial sensor based on a broad-side coupled SRR topology with a multi-layer substrate,” *Appl. Phys. A, Solids Surf.*, vol. 110, no. 1, pp. 189–197, Jan. 2013.

[46] J. Fraden, Handbook of Modern Sensors: Physics, Design, and Applications, 3rd ed. New York, NY, USA, Springer, 2004.

[47] J. Naqui, M. Durán-Sindreu and F. Martín, “Novel Sensors Based on the Symmetry Properties of Split Ring Resonators (SRRs),” Sensors, vol 11, pp. 7545í7553, 2011.

[48] Taha A. Elwi, “Further Investigation on Solant-Rectenna based Flexible Hilbert-Shaped Metamaterials”, *IET Nanodielectrics*, Volume 4, issue 12, pp. 1-12, March 2020.

[49] Taha A. Elwi and A. M. Al-Saegh, “Further realization of a flexible metamaterial based antenna on indium nickel oxide polymerized palm fiber substrates for RF energy harvesting”, *International Journal of Microwave and Wireless Technologies*, Cambridge, Volume 5, issue 4, pp. 1-9, May 2020.

[50] Turgul, V.; Kale, I. "Permittivity extraction of glucose solutions through artificial neural networks and non-invasive microwave glucose sensing". Sens. Actuators A Phys. Volume 277, 1 July 2018, Pages 65-72.

[51] I. Nadeem, D-Y. Choi, "Study on Mutual Coupling Reduction Technique for MIMO Antennas", IEEE Access (Volume: 7), December 2018, DOI: 10.1109/ACCESS.2018.2885558.

[52] J. Zhang, Y. Zhang, "Optimized Low-Power Flexible Magnetic-Coupling Antenna for Wearable Devices", IEEE Transactions on Antennas and Propagation (Volume: 67, Issue: 1, Jan. 2019). DOI: 10.1109/TAP.2018.2874799.

[53] Karamzadeh, S., V. Rafii, M. Kartal, O. N. Ucan, and Bal S. Virdee. "Circularly polarised array

antenna with cascade feed network for broadband application in C-band." Electronics Letters 50, no. 17, 2014.

[54] R.V. Hariprasad, D Vakula and M Chakravarthy, "A novel Fractal Slot DGS Microstrip Antenna for WIFI Application", IEEE Indian Conference on Antennas and Propagation, pp. 1-4, 2018.

[55] Lovepreet Singh and Mandeep Kaur, "Review of Microstrip Patch Antenna using Fractal Techniques for Wireless Application", International Journal of Engineering Trends and Technology, vol. 49, no. 6, July 2017.

[56] Y. Kumar; R. K.Gangwar; B. K. Kanaujia, "Characterization of CP Radiations in a Planar Monopole Antenna Using Tuning Fork Fractal Slot for LTE Band13/Wi-Max and Wi-Fi Applications", IEEE Access (Volume: 8), 09 July 2020. DOI: 10.1109/ACCESS.2020.3008285.

[57] H. Rajabloo, V. A. Kooshki and H. Oraizi, "Compact microstrip fractal Koch slot antenna with ELC coupling load for triple-band application", AEU-Int. J. Electron. Commun., vol. 73, pp. 144-149, Mar. 2017.

[58] B. B. Mandelbrot, "The Fractal Geometry of Nature", W. H. Freeman, San Francisco, CA, 1982.

[59] Bellido, Edson P., Gabriel D. Bernasconi, David Rossouw, Jérémy Butet, Olivier JF Martin, and Gianluigi A. Botton. "Self-Similarity of Plasmon Edge Modes on Koch Fractal Antennas." ACS nano 11, no. 11 (2017): 11240-11249.

[60] Jawad K. Ali, M. T. Yassen, M. R. Hussan, and A. J. Salim, " A Printed Fractal Based Slot Antenna for Multi-band Wireless Communication Applications", Progress In Electromagnetics Research, PIER Proceedings, Moscow, Russia, August 19-23, 2012.

[61] S. Akkole and N. Vasudevan, "Compact Multiband Microstrip Fractal Antenna Design for Wireless Applications –An Overview", (ICECA) IEEE, 28 December 2020, DOI: 10.1109/ICECA49313.2020.9297629..

[62] S. Akkole and N. Vasudevan, "Square microstrip Multiband fractal Antenna Using EBG Structure for Wireless Applications", International Journal of Pervasive Computing and Communications, pp. 1742-7371.31 March 2021.

[63] Fatima Ez-Zaki, Abdelilah Ghammaz and H. Belahrach, "Multiband Fractal Antenna for Wireless Applications", *IEEE 6th International Conference on Wireless Networks and Mobile communications*, 2019.

[64] Saurabh Kohli, Sukhwinder Singh Dhillon and Anupama Marwaha, "Design and Optimization of Multiband Fractal Microstrip Patch Antenna for Wireless Applications", 5th International Conference on Computational Intelligence and Communication Networks, 2013..

[65] D. Li, F. -S. Zhang, Z. -N. Zhao, L. -T. Ma, and X. -N. Li, " A CPW-fed Wideband Koch Snowflake Fractal Monopole for WLAN/WiMAX Applications", Progress In Electromagnetics Research C, PIER, Vol. 28, pp. 143-153, 2012.

[66] M. R. Haji-Hashemi, H. Mir-Mohammad Sadeghi, and V. M. Moghtadai, " Space-filling Patch Antennas with CPW Feed ", Progress In Electromagnetics Research Symposium, Cambridge, USA, March 26-29, 2006.

[67] P. S. Addison, "Fractals and Chaos", Institute of Physics Publishing, IOP, Ltd, London, 1997.

[68] Jawad K. Ali, "Microstrip-fed Printed Slot Antennas Based on Hilbert-Type Space-Filling Curves for Wireless Communication Systems", International Review on Modelling and Simulations, I.RE.MO.S, Vol. 3, No. 4, August 2010.

[69] Llorens-Quintana, Clara, and D. Robert Iskander. "Assessment of tear film using videokeratoscopy based on fractal dimension." Optometry and Vision Science 95, no. 1 (2018): 32-42.

[70] N. Poprzen, and M. Gacanovic, "Fractal Antennas: Design, Characteristics and Application ", Regular Paper, 2000.

[71] Bryson, Arthur Earl. Applied optimal control: optimization, estimation and control. Routledge, 2018.

[72] Natanson, Isidor Pavlovich. Theory of functions of a real variable. Courier Dover Publications, 2016.

[73] K. Falconar, "Fractal Geometry", John Wiley & Sons, Ltd., Baffins Lane, Chichister, 1990.

[74] Boiangiu, C., Adrian G. Morosan, and Marian Stan. "A fractal world: building visually-rich and fully-realistic natural environments." Int. J. Math. Comput. Simul 10 (2016): 100-111.

[75] Bellido, Edson P., Gabriel D. Bernasconi, David Rossouw, Jérémy Butet, Olivier JF Martin, and Gianluigi A. Botton. "Self-Similarity of Plasmon Edge Modes on Koch Fractal Antennas." ACS nano 11, no. 11 (2017): 11240-11249.

[76] Fang, Sizhen, Dylan A. King, Eun Bi Lee, and Robert S. Strichartz. "Spectral decimation for

families of self-Similar symmetric Laplacians on the Sierpinski gasket." arXiv preprint arXiv:1709.02031 (2017).

[77] Bannink, Tom, and Harry Buhrman. "Quantum Pascal's Triangle and Sierpinski's carpet." arXiv preprint arXiv:1708.07429 (2017).

[78] Cao, Thanh Nghia, and Wojciech J. Krzysztofik. "Hybrid Minkowski fractal island antenna operating in two bands of GPS satellite system." In 2016 IEEE International Symposium on Antennas and Propagation (APSURSI), pp. 211-212. IEEE, 2016.

[79] Chowdary, P. Satish Rama, A. Mallikarjuna Prasad, P. Mallikarjuna Rao, and Jaume Anguera. "Design and performance study of Sierpinski fractal-based patch antennas for multiband and miniaturization characteristics." Wireless Personal Communications 83, no. 3 (2015): 1713-1730.

[80] John McVay and Ahmad Hoorfar, "Miniaturization of top-loaded monopole antennas using Peano-curves." 2007 IEEE Radio and Wireless Symposium, CA, USA, DOI: 10.1109/RWS.2007.351816.

[81] M. R. I. Faruque, M. T. Islam, and N. Misran, "Design analysis of new metamaterial for EM absorption reduction," Progress in Electromagnetics Research, vol. 124, pp. 119–135, 2012, doi:10.2528/PIER11112301.

[82] H. Nakano, Low-Profile Natural and Metamaterial Antennas, Hoboken, NJ, USA:Wiley, 2016.

[83] Engheta, N., & Ziolkowski, R. W. (2007). Electromagnetic metamaterials: Physics and engineering explorations. New York: Wiley.

[84] B.Hazarika, B.Basu, and A.Nandi, "Design of Dual-Band Conformal AMC Integrated Antenna for SAR Reduction in WBAN," *Progress In Electromagnetics Research C*, Vol. 110, 91-102, 2021, doi:10.2528/PIERC20121202.

[85] Hasar UC, Buldu G, Kaya Y, Ozturk G, "Determination of Effective Constitutive Parameters of Inhomogeneous Metamaterials with Bianisotropy," IEEE Trans Microw Theory Tech, Volume: 66, Issue: 8, Aug. 2018, DOI: 10.1109/TMTT.2018.2846726.

[86] M. Mezher, M. Ilyas, O. Bayat, and Q. H. Abbasi, "Bit Error Rate Performance of In-vivo Radio Channel Using Maximum Likelihood Sequence Estimation," International

Conference on Electrical, Communication, and Computer Engineering (ICECCE), 28 August 2020, Istanbul, Turkey.

[87] A T. Zerith M and M. Nesasudha, “A Compact Wearable 2.45 GHz Antenna for WBAN Applications,” IEEE (2020) 5th International Conference on Devices, Circuits and Systems (ICDCS), 23 April 2020, India.

[88] Arif A, Akram MR, Riaz K, Zubair M and Mehmood MQ, “Koch Fractal Based Wearable Antenna Backed with EBG Plane,” (2020) IEEE 17th International Bhurban Conference on Applied Sciences and Technology (IBCAST), Pakistan.

[89] E. Cil and S. Dumanli,” The Design of a Reconfigurable Slot Antenna Printed on Glass for Wearable Applications,” IEEE Access, 20 May, 2020, DOI: 10.1109/ACCESS.2020.2996020.

[90] Al-Dulaimi, Z., T. A. Elwi, and D. C. Atilla, "Design of a meander line monopole antenna array based hilbert-shaped reject band structure for MIMO applications," IETE Journal of Research, Vol. 66, 1-10, 2020. doi:10.1080/03772063.2020.1743207.

[91] Al Naiemy, Y., T. A. Elwi, and L. Nagy, "An end fire printed monopole antenna based on electromagnetic band gap structure," Automatika, Vol. 61, No. 3, 482-495, 2020, doi:10.1080/00051144.2020.1785783.

[92] Al Naiemy, Y, and L. Nagy,” Improved Antenna Gain and Efficiency Using Novel EBG Layer,” 2020 IEEE 15th International Conference of System of Systems Engineering (SoSE), 01 July, Hungary, DOI: 10.1109/SoSE50414.2020.9130494.

[93] Dassault Systèmes "CST Microwave Studio", [computer program] Available at: http://www.cst.com [Accessed: 11 January 2019.

[94] A. Abohmra, S. Ramani, A. Sharif, M. A. Imran, Q. Abbasi, W. Ahmad, “Novel Flexible and Wearable 2.4 GHz Antenna for Body-Centric Applications,” 2019 IEEE Intl Conf on Dependable, 04 November, Japan, DOI: 10.1109/DASC/PiCom/CBDCom/CyberSciTech.2019.00082.

[95] L. Belrhiti, F. Riouch, A. Tribak, J. Terhzaz, and A. M. Sanchez, Flexible Antennas Design and Test for Human Body Applications Scenarios, J. Microwaves, Optoelectron.

Electromagn. Appl., vol. 16, no. 2, pp. 494513, 2017.

[96] Al Naiemy, Y., T. A. Elwi, and L. Nagy, “Enhancing the Microstrip Antenna Gain Using a Novel EBG Lens Based on a Single Layer,” (2018) IEEE 11th International Symposium on Communication Systems, Networks & Digital Signal Processing (CSNDSP), 27 September, Hungary, DOI: 10.1109/CSNDSP.2018.8471786.

[97] Khaleel, Haider R., Hussain M. Al-Rizzo, and Ayman I. Abbosh. ”Design, fabrication, and testing of flexible antennas.” In Advancement in Microstrip Antennas with Recent Applications. IntechOpen, 2013.

[98] Jafargholi A, Jafargholi A, Choi JH, “Mutual Coupling Reduction in an Array of Patch Antennas Using CLL Metamaterial Superstrate for MIMO Applications,” IEEE Trans Antennas Propag. Volume: 67, Issue: 1, Jan. 2019, DOI: 10.1109/TAP.2018.2874747.

[99] Al-Sabbagh HM, Elwi TA, Al-Naiemy Y and Al-Rizzo HM, ”A compact triple-band metamaterial-inspired antenna for wearable applications,” Microwave and Optical Technology Letters, 04 October 2019.

[100] Y. Alnaiemy, and L. Nagy, “Design of a Controllable Antenna Based on Embedded Differential PSK Modulation,” Progress In Electromagnetics Research, Vol. 90, 43-62, 2021. Doi:10.2528/PIERB20100106.

[101] Erdem Cil and Sema Dumanli, "The Design of a Reconfigurable Slot Antenna Printed on Glass for Wearable Applications", IEEE Access (Volume: 8), 20 May 2020, DOI: 10.1109/ACCESS.2020.2996020.